Biol. Cybern. 75, 361–379 (1996)

Biological Cybernetics

A kinetic mechanism for nicotinic acetylcholine receptors based on multiple allosteric transitions

Stuart J. Edelstein [1,2], Olivier Schaad [1], Eric Henry [3], Daniel Bertrand [4], Jean-Pierre Changeux [2]

[1] Département de Biochimie, Université de Genève, CH-1211 Geneva 4, Switzerland
[2] Neurobiologie Moléculaire, Institut Pasteur, F-75734 Paris Cedex 15, France
[3] Laboratory of Chemical Physics, NIDDK, NIH, Bethesda, MD 20892, USA
[4] Départment de Physiologie, Université de Genève, CH-1211 Geneva 4, Switzerland

Received: 22 November 1995/Accepted in revised form: 24 July 1996

Abstract. Nicotinic acetylcholine receptors are transmembrane oligomeric proteins that mediate interconversions between open and closed channel states under the control of neurotransmitters. Fast in vitro chemical kinetics and in vivo electrophysiological recordings are consistent with the following multi-step scheme. Upon binding of agonists, receptor molecules in the closed but activatable resting state (the Basal state, B) undergo rapid transitions to states of higher affinities with either open channels (the Active state, A) or closed channels (the initial Inactivatable and fully Desensitized states, I and D). In order to represent the functional properties of such receptors, we have developed a kinetic model that links conformational interconversion rates to agonist binding and extends the general principles of the Monod-Wyman-Changeux model of allosteric transitions. The crucial assumption is that the linkage is controlled by the position of the interconversion transition states on a hypothetical linear reaction coordinate. Application of the model to the peripheral nicotinic acetylcholine receptor (nAChR) accounts for the main properties of ligand-gating, including single-channel events, and several new relationships are predicted. Kinetic simulations reveal errors inherent in using the dose-response analysis, but justify its application under defined conditions. The model predicts that (in order to overcome the intrinsic stability of the B state and to produce the appropriate cooperativity) channel activation is driven by an A state with a K_d in the 50 nM range, hence some 140-fold stronger than the apparent affinity of the open state deduced previously. According to the model, recovery from the desensitized states may occur via rapid transit through the A state with minimal channel opening, thus without necessarily undergoing a distinct recovery pathway, as assumed in the standard 'cyclic' model. Transitions to the desensitized states by low concentration 'pre-pulses' are predicted to occur without significant channel opening, but equilibrium values of IC_{50} can be obtained only with long pre-pulse times. Predictions are also made concerning allosteric effectors and their possible role in coincidence detection. In terms of future developments, the analysis presented here provides a physical basis for constructing more biologically realistic models of synaptic modulation that may be applied to artificial neural networks.

Correspondence to: S. Edelstein, 30 quai Ernest-Ansermet, CH-1211 Geneva 4, Switzerland (Tel. (+41-22) 702-6486, fax: (+41-22) 702-6476, e-mail: Stuart.Edelstein@biochem.unige.ch)

1 Introduction

Rapid chemical communications at the synapses of neuromuscular junctions or between neurons occur via the quantal release into the synaptic cleft of neurotransmitter molecules in 'pulses' of millimolar concentration and millisecond duration (Kuffler and Yoshikami 1975; Clements et al. 1992). The post-synaptic membrane contains a high density of ionotropic receptor (ligand-gated channel), present mainly in closed states prior to neurotransmitter release, but capable of interconverting rapidly upon binding of neurotransmitter to an open state with a permeable ion channel. However, the open state is transient and closure occurs either by returning to the initial state (following a brief pulse of neurotransmitter, as commonly occurs under physiological conditions) or by converting to desensitized states (when neurotransmitters or other modulators are present for longer times).

Evidence from studies both in vitro and in vivo indicates that even after brief pulses, small, but finite amounts of the receptor population remain in desensitized states (Magleby and Pallotta 1981; Colquhoun et al. 1992; Hestrin 1993), thereby constituting a short-term remembrance of the transient opening. Desensitization can also be achieved by low concentrations (less than micromolar) of neurotransmitters (Katz and Thesleff 1957; Trussell and Fischbach 1989; Colquhoun et al.

1992; Hestrin 1993; Franke et al. 1993) in the range of ambient extracellular concentrations (Katz and Miledi 1977; Kanai et al. 1993), suggesting that partial desensitization may be a common factor in modulating synaptic efficacy, with implications for short-term memory (Changeux and Heidmann 1987), the mechanisms of modulator actions (Léna and Changeux 1993; Galzi and Changeux 1994), and possible influences of volume transmission (Fuxe and Agnati 1991).

Although considerable information is now available for several classes of ionotropic receptors for other neurotransmitters (Galzi and Changeux 1994), the studies are most advanced for the acetylcholine receptor (AChR), at the level of both structure and function. The former include extensive mapping of ligand binding and ion channel sites (review by Changeux et al. 1992), as well as information on the three-dimensional structure at 0.9 nm resolution (Unwin 1993). The latter comprise a large body of dose-response analyses that reveal the cooperative nature of the agonist-receptor interactions (Katz and Thesleff 1957), as well as single-channel measurements that provide kinetic rate constants for several steps in ligand-gating (see Sakmann et al., 1980; review by Lingle et al. 1992). Additional insights are provided by mutant forms of the neuronal AChR receptors, such as the $\alpha 7$ mutant L247T with high-affinity, non-desensitizing currents, and unconventional pharmacology (Revah et al. 1991; Bertrand et al. 1992).

Concerning cooperative ligand binding, in the case of oligomeric proteins the Monod-Wyman-Changeux theory (Monod et al. 1965) posits that cooperative binding results from the differential stabilization of discrete symmetric states from pre-existing conformational equilibria. This theory has had a powerful effect on the understanding of cooperative interactions for haemoglobin and allosteric enzymes (Edelstein 1975; Shulman et al. 1975; Perutz 1989). The allosteric approach has been extended in general terms to membrane receptors for neurotransmitters (Changeux et al. 1967; Karlin 1967; Edelstein 1972; Dionne et al. 1978; Heidmann and Changeux 1979; Changeux, 1990; Jackson 1989; Galzi and Changeux 1994), and the existence of allosteric transitions is supported by spontaneous channel openings (Jackson 1986), as well as significant levels of desensitized states for *Torpedo* receptor in the absence of agonist (Heidmann and Changeux 1979; Boyd and Cohen 1980; Prinz and Maelicke 1992). Although the allosteric theory has been applied to certain features of the AChR (review by Changeux 1990), a full interpretation of the kinetic behaviour of the AChR in terms of allosteric states requires additional theoretical developments in order to link the rates of interconversion between conformational states to the extent of ligand binding. Otherwise, as concluded by earlier investigators (Colquhoun and Hawkes 1977), 'the number of rate constants involved is too large for the theory be applied'. A linear free-energy relationship (Leffler 1953; Szabo 1978; Jencks 1985; Eaton et al. 1991) is presented here that permits characterization of the transition state for the interconversion between two conformations in terms of its position on a hypothetical linear reaction coordinate. The position determines the effect of ligand binding on the interconversion rates, thereby limiting the degrees of freedom in the assignment of values to the rate constants.

The theory is applied to several features of the nicotinic acetylcholine receptor (nAChR) and provides a number of advantages, notably in explaining how channels may remain silent during recovery without invoking a special pathway as in the standard cyclic model (Katz and Thesleff 1957; Colquhoun and Sakmann 1985; Franke et al. 1993). In addition, the explicit analysis of receptor activation and desensitization in terms of discrete conformational states provides biologically consistent elementary mechanisms for developing models of neural networks. While many models based on formal neurons (McCulloch and Pitts 1943) have been proposed (Amit, 1989; Churchland and Sejnowski, 1992), in only a limited number of cases have synaptic modulations been related to the regulatory properties of the relevant ligand-gated (Heidmann and Changeux 1982; Dehaene et al. 1987; Changeux and Dehaene 1989; Changeux 1993) or voltage-gated (Finkel and Edelman 1985) ion channels. By extending the allosteric theory to a full kinetic description of receptor interconversions between activatable, active and closed conformations, molecular mechanisms can now be formulated for both Hebbian plasticity within the context of synaptic triads (review by Changeux 1993) and coincidence detection by allosteric effects that offer a novel paradigm in addition to (or as an alternative to) that established on the basis of the *N*-methyl-D-aspartate (NMDA) receptor channel properties (see Discussion).

2 Biological premises

The functional model for the nAChR is based on experimental evidence from various sources (for reviews see Changeux 1990; Karlin 1991; Role 1992; Sargent 1993; Galzi and Changeux 1994; Blanton and Cohen 1994).

(1) The nAChR is a transmembrane hetero-pentamer, with a $[2\alpha{:}1\beta{:}1\gamma/\varepsilon{:}1\delta]$ or $[2\alpha_i{:}3\beta_j]$ stoichiometry for the junctional or neuronal receptors, respectively, organized around a pseudo-rotational axis of symmetry perpendicular to the plane of the membrane which coincides with the ion channel lined by the M2 transmembrane segment.
(2) Agonist binding sites are present on α subunits, with adjacent non-α subunits contributing to non-equivalence in the affinity for certain ligands, particularly antagonists, but with effective equivalence for agonists generally observed (Changeux and Edelstein 1994), apart from two reports of marked heterogeneity (Jackson 1988; Sine et al. 1990).
(3) The receptor molecules are present in an equilibrium between a number of distinct conformational states (at least four: B, A, I and D) which differ by their affinity for agonists (and antagonists) and the rates at which they interconvert. One of the states (A) occurs with an open channel, with an intrinsic conductance and mean open time in single channel recordings.

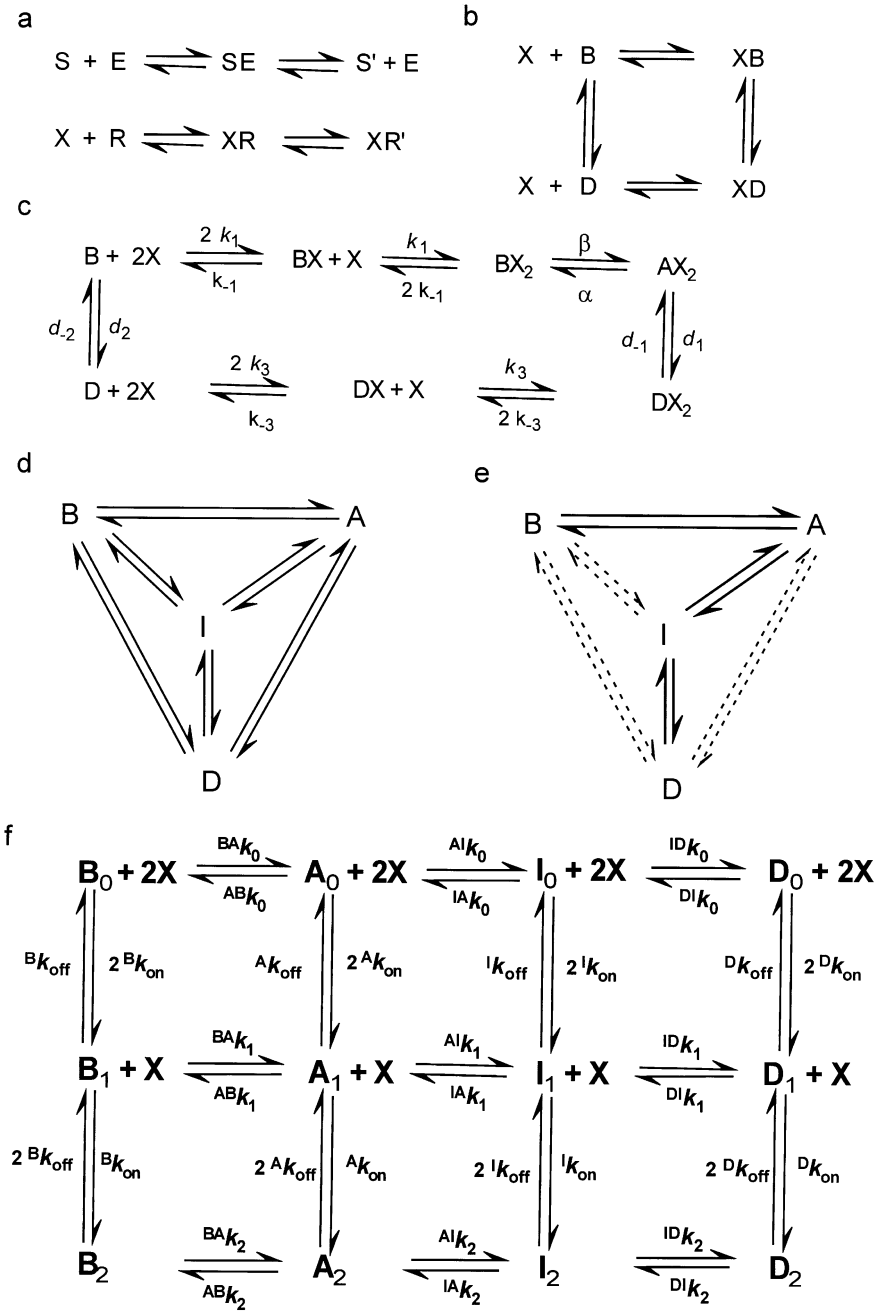

Fig. 1a–f. Mechanistic descriptions of receptor ligand interactions. **a** The parallel drawn by del Castillo & Katz (1957) between enzyme-substrate interactions and receptor-ligand interactions. In their original formulations, the ligand was also abbreviated 'S', with reference to acetylcholine, substrate for the acetylcholine esterase, but here 'X' is used to indicate the ligand bound to the receptor for consistency with the other mechanisms depicted in this figure. **b** The cyclic model as formulated by Katz and Thesleff (1957). In their original scheme, the ligand was represented by 'S' and the two states were indicated by 'A' and 'B', but since these letters have other meanings in the mechanisms that follow, we have replaced them here by 'X', 'B' and 'D', respectively. **c** The recent version of the cyclic scheme of Katz and Thesleff (1957), as presented by Franke et al. (1993), to incorporate the presence of two ligand-binding sites on each receptor. **d** All potential interactions among the four allosteric states detected by Heidmann and Changeux (1980), as indicated by the arrangement at the vertices of a tetrahedron. The low-affinity resting state (previously designated 'R') is here designated 'B' (for Basal) to avoid confusion with the high affinity (relaxed) state, 'R' in the original formulation of Monod et al. (1965). **e** Linear simplification of the interactions of the four states corresponding to the pathway selected to follow the lowest transition state barriers. **f** Complete network of rate constants for conformational interconversions and agonist binding at two sites on each receptor. Each *column* corresponds to a series of ligand binding events at two identical sites per receptor, with the rates specified along the *vertical arrows* by the state-specific intrinsic 'on' and 'off' constants, with statistical factors included. Each row corresponds to a series of transitions between states governed by rate constants that vary with the number of ligand molecules bound (i = 0, 1 or 2), with the initial and final states in the *superscript* and the number of ligands in the *subscript*

(4) Interconversions between conformational states occur freely, whether or not agonist is bound, as indicated by spontaneous interconversions to A or D in the absence of ligand.

3 Description of the model

3.1 Interconversion cascade between multiple conformational states

Functional models for nAChR kinetics have been developed in the last decades that followed the progress in knowledge of the properties of the receptor molecule (Fig. 1). Early descriptions (del Castillo and Katz 1957) recognized the similarity between enzyme-substrate interactions and receptor-ligand interactions (Fig. 1a). This formulation was further elaborated to account for desensitization (Katz and Thesleff 1957), leading to the cyclic reaction scheme (Fig. 1b), with distinct resting and desensitized states present in the absence of agonist, anticipating in this respect the allosteric theory. The cyclic reaction pattern was subsequently expanded to incorporate the two agonist binding sites (Fig. 1c), and remains the model generally employed for analysing kinetic data (Colquhoun and Sakmann 1985; Franke et al. 1993). To

account for in vitro fast kinetic observations on ligand binding and ion channel opening with *Torpedo* receptors (Heidmann and Changeux 1980; Neubig and Cohen 1980; Changeux, 1990) four conformational states, B, A, I and D, were postulated, with an interconversion pattern that corresponds to the vertices of a tetrahedron (Fig. 1d). According to this scheme, all interaction pathways are in principle possible, but they could conceivably be limited by structural or kinetic constraints of the receptor that render obligatory a certain order of passage between states.

A new and simplified form of the tetrahedral model is presented here, based on a predominant kinetic pathway, as indicated in Fig. 1e, that corresponds to the passage between states over the lowest transition state barriers. When the secondary pathways (indicated by dotted arrows) can be neglected, the tetrahedral arrangement reduces to the linear cascade $B \rightleftharpoons A \rightleftharpoons I \rightleftharpoons D$. (The reasons that justify such a linear cascade under certain conditions are presented in the Discussion.) The linear cascade permits a full description of all ligand-binding and conformation transition rates in a two-dimensional kinetic network (Fig. 1f), with ligand (agonist) reactions represented vertically and conformational interconversion reactions represented horizontally. The ratios of the various ligand binding and interconversion rate constants define the equilibrium parameters summarized in Fig. 2a for the overlapping reaction cycles associated with the ligand binding to the three pairs of states.

3.2 Linkage between ligand binding and the rates of interconversion between allosteric states established by a transition state positional parameter

Since the affinity for agonist differs between the partners of each pair of states, as indicated by the affinity ratios ${}^{BA}c$, ${}^{AI}c$, and ${}^{ID}c$, defined in Fig. 2a, equation set (i), each step of ligand binding produces a decrease in the allosteric equilibrium constants ${}^{BA}L_i$, ${}^{AI}L_i$, and ${}^{ID}L_i$ by the corresponding affinity ratio, as indicated in Fig. 2a, equation set (ii). Changes in the rates of interconversion of the allosteric states must also occur with each step of ligand binding, as indicated by the relationships of Fig. 2a, equation set (iii). Specifically, the stabilization of the higher-affinity member of each pair of states resulting from the binding of one molecule of agonist is reflected by a decreasing interconversion rate towards the lower affinity state and/or an increasing interconversion rate towards the higher-affinity state. For example, progression from ${}^{BA}L_{i-1}$ to ${}^{BA}L_i$ must correspond to ${}^{AB}k_i / {}^{AB}k_{i-1} < 1$ and/or ${}^{BA}k_i / {}^{BA}k_{i-1} > 1$.

In order to implement a general theory for the linkage of conformational interconversion rates and ligand binding, we assume that the transition state for each interconversion will be stabilized by ligands. The extent of this stabilization is assumed to be intermediate with respect to the effects of the ligands on each on the two participating allosteric states and weighted toward the properties of the allosteric state that the transition state more closely resembles. This assumption may be expressed quantitatively in terms of the *position of the transition state on a hypothetical reaction coordinate*. In this case, for each pair of states a positional parameter is defined (${}^{BA}p$, ${}^{AI}p$, or ${}^{ID}p$), as presented in Fig. 2b, that characterizes the transition state on a linear scale between 0 and 1 in terms of its proximity to the lower affinity state of the pair. Each positional parameter, in the exponent, determines the contributions of interconversion rate changes to the corresponding affinity ratio, as defined in Fig 2b, equation sets (iv) and (v).

The transition state positional parameter thus predicts a systematic variation in the interconversion rates with ligand binding. For example, with a value of ${}^{BA}c = 0.001$, ${}^{BA}L_i$ decreases by 10^3 for each ligand bound and this change must be reflected by a corresponding increase in the $B \rightarrow A$ rates, a corresponding decrease in the $A \rightarrow B$ rates, or (as is more likely) a combination of the two. The transition state positional parameter permits a weighting of the changes in the $A \rightarrow B$ and $B \rightarrow A$ rates. For a positional parameter of ${}^{BA}p = 0.5$, each ligand binding step would increase the $B \rightarrow A$ rate and decrease the $A \rightarrow B$ rate by $\sqrt{{}^{BA}c}$, whereas lower values imply greater changes in the $B \rightarrow A$ rates than in the $A \rightarrow B$ rates (Table 1).

The linkage defined in Fig. 2b corresponds to a linear free energy relationship concerning the proximity of the transition state to the product and reactant states, such that the logarithm of the rate constants exhibits a linear dependence on the equilibrium constants (Leffler 1953; Fersht et al. 1986). Such a linear relationship satisfactorily represents the kinetics of the interconversions between allosteric states for haemoglobin (Sawicki and Gibson 1976; Szabo 1978; Eaton et al. 1991) over a wide range of rates. Use of the free energy relationships reduced the number of parameters necessary to define the interconversion rate constants by a factor of 2 (with two agonist binding sites), increasing to a factor of 4 in the case of five agonist binding sites.

3.3 Pathway selection for changes of state are determined by energy barriers for interconversions within the allosteric cascade

The various relationships linking ligand binding, allosteric equilibria, and transition state barriers define a free energy profile, as presented in Fig. 3. The profile corresponds to values of the parameters of the model derived mainly from mouse muscle with rapid agonist application (Franke et al. 1993), as summarized in Table 1. The vertical ladders for each state and the intervening transition states correspond to the change in free energy for each molecule of agonist bound. Hence the step sizes for the B, A, I and D states increase with affinity according to the series of dissociation constants ${}^{B}K_d > {}^{A}K_d > {}^{I}K_d > {}^{D}K_d$. The vertical alignment of the ladder for each state is set by the values assigned to the relative concentrations of B_0, A_0, I_0, and D_0. The transition state heights are determined by the positional parameters (Fig. 2b). The progression of doubly-liganded states $B_2 \rightarrow A_2 \rightarrow I_2 \rightarrow D_2$ represents the allosteric cascade for the conformational changes elicited by application of

a

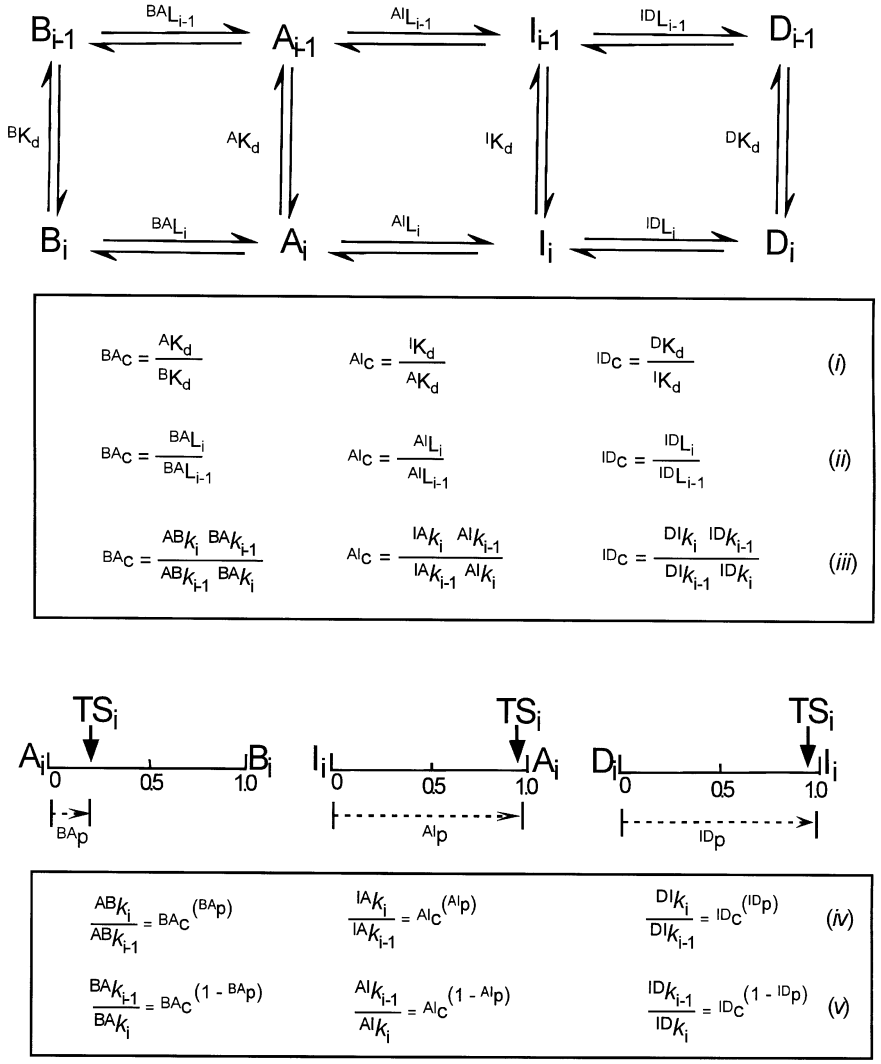

b

Fig. 2a, b. Linkage relationships involving ligand binding, rates of interconversion between allosteric states, and transition state properties. **a** Equilibrium parameters specified by the rate constants and the changes produced by binding the i-th molecule of ligand. Three overlapping reaction cycles are presented for the B–A, A–I, and I–D pairs of states upon addition of the i-th ligand. For each pair of states, the allosteric equilibrium constants ($^{BA}L_i$, $^{AI}L_i$, and $^{ID}L_i$) are defined as the ratio of the concentrations of the lower and higher affinity partners at each stage of ligand binding (indicated by i = 0, 1 or 2), e.g. $^{BA}L_1 = [B_1]/[A_1]$. The values of these constants at each i are specified by the ratio of the corresponding transition rate constants (as defined in Fig. 1f), e.g. $^{BA}L_1 = {}^{AB}k_1/{}^{BA}k_1$. Changes in allosteric constants from one row to the next are controlled for each pair of states by the ligand-affinity ratios (^{BA}c, ^{AI}c, or ^{ID}c), as specified by equation set (i), e.g. $^{BA}c = {}^{A}K_d/{}^{B}K_d$, where the intrinsic ligand binding equilibrium constants are defined by the ratio of the off and on rates, e.g. $^{B}K_d = {}^{B}k_{off}/{}^{B}k_{on}$ (see Fig. 1f). These values fix the change in the corresponding allosteric equilibrium with each ligand binding event according to equation set (ii), e.g. $^{BA}c = {}^{BA}L_1/{}^{BA}L_0$. Since the allosteric equilibrium constants can be replaced by the ratio of the corresponding interconversion rate constants, e.g. $^{BA}L_i/{}^{BA}L_{i-1} = ({}^{AB}k_i/{}^{BA}k_i)/({}^{AB}k_{i-1}/{}^{BA}k_{i-1})$, the affinity ratios can also be expressed in terms of ratios of the interconversion rate constants, as presented (after rearrangement) in the equation set (iii). **b** Transition state positions and linkage to interconversion rates. For each pair of states, a hypothetical linear reaction coordinate from 0 to 1 is established such that each transition state may be characterized by its proximity to the parent state with lower affinity, as specified by the transition state positional parameters ^{BA}p, ^{AI}p, and ^{ID}p, with values in the diagrams of the three pairs of states as assigned in Table 1. The overall dependence of the interconversion rates on ligand binding is indicated for each pair of states by the equation sets (iv) and (v), expressing the effects of the transition state positional parameters on the rates towards the lower-affinity state (iv) or towards the higher- affinity state (v). Hence, for each pair of states, the product of (iv) and (v) equals (iii). It should be emphasized that the transition state positional parameters describe the relative stabilization by ligand, but not the absolute heights on a free energy scale, the latter being determined by specific kinetic features (see Fig. 3)

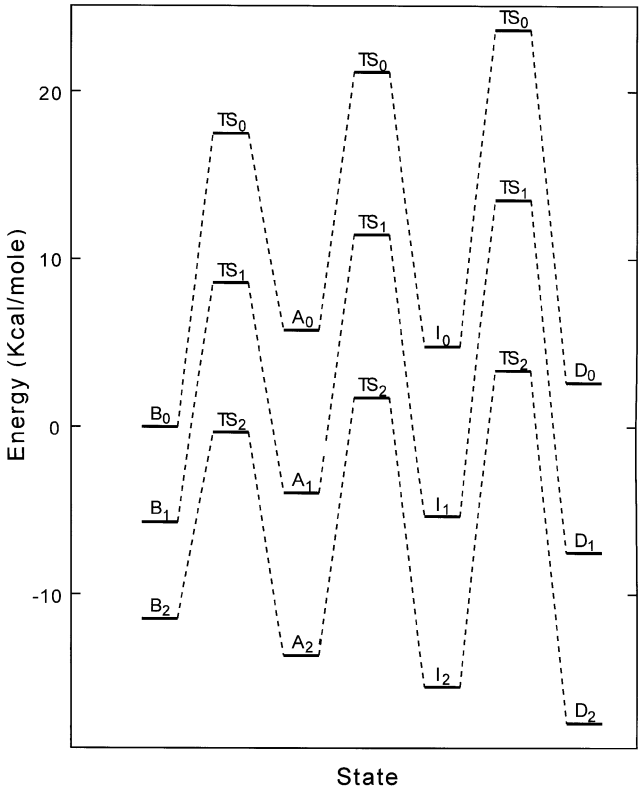

Fig. 3. Free energy diagram for the four-state allosteric model, including all liganded and unliganded allosteric states, as well as their respective transition states. The B, A, I, and D states are each represented by a free energy ladder with step size for each ladder determined by $\Delta G = -RT \ln {}^{X}K_d$, where ${}^{X}K_d$ is the intrinsic ligand dissociation constant (${}^{B}K_d$, ${}^{A}K_d$, ${}^{I}K_d$, or ${}^{D}K_d$). The vertical position of each ladder is set by $\Delta G = 0$ for B_0 and for the successive states by $\Delta G = -RT \ln {}^{XY}L_0$, where ${}^{XY}L_0$ is the allosteric constant (${}^{BA}L_0$, ${}^{AI}L_0$, or ${}^{ID}L_0$). The transition states are placed according to the free energy of activation $\Delta G^{\ddagger}$, derived from transition state theory as expressed by the equation: $k = \kappa(k_B T/h)e^{-\Delta G^{\ddagger}/RT}$, where κ is the transmission constant (which can be assumed to equal 1.0 if there are no barrier recrossings), k_B is Boltzman's constant, h is Planck's constant, R is the gas constant, and T is the absolute temperature (Steinfeld et al. 1989). For the interconversions between states, the rates for the doubly-liganded forms are specified on the basis of the experimental data, as summarized in Table 1. The changes in the rates for the unliganded and singly-liganded forms are determined by the transition state positional parameters, as defined in Fig. 2b. For example, with ${}^{BA}p = 0.2$, it can be seen that the vertical spacing of the transition states for the $B_i \rightleftharpoons A_i$ interconversions at different degrees of ligand binding more closely resemble the spacing between the A_i forms than the spacing between the B_i forms

a strong and prolonged pulse of agonist, with the time of passage through A_2 corresponding to the average open time in single-channel measurements. Following termination of the pulse, agonist dissociation drives the system to the unliganded states and the initial distribution is re-established relatively rapidly, particularly from I_2 along the pathway $I_2 \rightarrow I_1 \rightarrow I_0 \rightarrow A_0 \rightarrow B_0$. In this case, passage through A_0 is extremely rapid, as described in Sect. 5 (see Fig. 4b), since the barrier from I_0 is much higher than the barrier to B_0, thereby providing an explanation of recovery with minimal channel opening without requiring a distinct cycle as in the standard models (Katz and Thesleff 1957; Colquhoun and Sakmann 1985; Franke et al. 1993).

4 Formalization of the model

4.1 Equilibrium processes

The standard allosteric equations (Monod et al. 1965; Rubin and Changeux 1966) may be expanded to include all four states for ($\bar{Y}_4$), a global ligand-binding function, and ($\bar{D}$), the fractional occupancy of the D state, as described in the Appendix (A1 and A2). For the simulation of response curves as a function of ligand concentration and their relation to ligand binding, the $B \rightleftharpoons A$ transitions are of primary interest and for these two states, the relevant functions are fractional ligand binding ($\bar{Y}_{BA}$) and normalized fractional occupancy of the A state ($\bar{A}_{norm}$), as defined by (A3) and (A6), respectively. The occupancy function is normalized in order to expand its values to the range 0–1. The cooperative behaviour of the system is defined independently for the binding and change of state functions in terms of distinct Hill coefficients, $n_{H,Y}$ and $n_{H,A}$ (A7 and A8). For simulations of the desensitization arising from preincubation of receptor at concentrations of ligand too low to trigger significant channel opening (see Fig. 9 below), the equation describing the normalized occupancy of the D state, $\bar{D}_{norm}$ (A11), is employed.

4.2 Transient processes

The model has been implemented to study the time-dependent properties for both 'molecular events' (as observed for the stochastic properties of an individual receptor in single channel measurements) and the 'macroscopic' data (as observed for the composite average of a population of molecules). In principle, the two approaches converge when sufficient numbers of molecular events are available to establish mean values that can be related to apparent macroscopic rate constants (Magleby and Stevens 1972; Sakmann et al. 1980; Frenkel, 1993). Therefore, we have developed programs to simulate both the molecular and macroscopic processes. For single-channel simulations, the matrix of kinetic constants is converted to transition probabilities per unit time in a stochastic algorithm which involves direct calculation of lifetimes of each event (Steinfeld et al. 1989). This latter approach (with details of the method presented in the legend to Fig. 5) reduces calculation times by several orders of magnitude compared with methods that use a fixed Δt interval (Cox and Miller 1965; Wilson and Brown 1985; Bertrand et al. 1989). The kinetic simulations of populations of molecules are performed by assigning values for the basic parameter set, formulating the appropriate differential equations in matrix representation, and solving the system at a selected concentration of agonist by making use of the Livermore solver (LSODA) for ordinary differential equations with automatic method switching for stiff and non-stiff problems (Petzold 1983). A comparison of the results obtained with

Table 1. Parameter values for the four-state allosteric kinetic mechanism

A. *State parameters*:	B state	A state	I state	D state
Independent parameters				
Ligand on rates ($M^{-1}s^{-1}$):	${}^{B}k_{on} = 1.5 \times 10^{8}$	${}^{A}k_{on} = 1.5 \times 10^{8}$	${}^{I}k_{on} = 1.5 \times 10^{8}$	${}^{D}k_{on} = 1.5 \times 10^{8}$
Ligand off rates (s^{-1}):	${}^{B}k_{off} = 8000$	${}^{A}k_{off} = 8.64$	${}^{I}k_{off} = 4.0$	${}^{D}k_{off} = 4.0$
Deduced parameters				
Equilibrium constants (M):	${}^{B}K_{d} = 5.3 \times 10^{-5}$	${}^{A}K_{d} = 5.7 \times 10^{-8}$	${}^{I}K_{d} = 2.7 \times 10^{-8}$	${}^{D}K_{d} = 2.7 \times 10^{-8}$
Affinity ratios:	${}^{BA}c = 1.08 \times 10^{-3}$	${}^{AI}c = 0.46$	${}^{ID}c = 1.0$	

B. *Interconversion parameters*:	B ↔ A	A ↔ I	I ↔ D
Independent parameters			
TS positional parameter:	${}^{BA}p = 0.2$	${}^{AI}p = 0.99$	${}^{ID}p = 0.99$
Interconversion rates (s^{-1}):	${}^{BA}k_{2} = 3.0 \times 10^{4}$	${}^{AI}k_{2} = 20.0$	${}^{ID}k_{2} = 5.0 \times 10^{-2}$
	${}^{AB}k_{2} = 7.0 \times 10^{2}$	${}^{IA}k_{2} = 0.81$	${}^{DI}k_{2} = 1.2 \times 10^{-3}$
Deduced parameters			
Interconversion rates (s^{-1}):	${}^{BA}k_{0} = 0.54$	${}^{AI}k_{0} = 19.7$	${}^{ID}k_{0} = 5.0 \times 10^{-2}$
	${}^{AB}k_{0} = 1.08 \times 10^{4}$	${}^{IA}k_{0} = 3.74$	${}^{DI}k_{0} = 1.2 \times 10^{-3}$
	${}^{BA}k_{1} = 1.3 \times 10^{2}$	${}^{AI}k_{1} = 19.85$	${}^{ID}k_{1} = 5.0 \times 10^{-2}$
	${}^{AB}k_{1} = 2.74 \times 10^{3}$	${}^{IA}k_{1} = 1.74$	${}^{DI}k_{1} = 1.2 \times 10^{-3}$
Allosteric constants:	${}^{BA}L_{0} = 2 \times 10^{4}$	${}^{AI}L_{0} = 0.19$	${}^{ID}L_{0} = 2.5 \times 10^{-2}$
	${}^{BA}L_{1} = 21.6$	${}^{AI}L_{1} = 8.7 \times 10^{-2}$	${}^{ID}L_{1} = 2.5 \times 10^{-2}$
	${}^{BA}L_{2} = 2.3 \times 10^{-2}$	${}^{AI}L_{2} = 4.0 \times 10^{-2}$	${}^{ID}L_{2} = 2.5 \times 10^{-2}$

For the 14 independent rate constants (four on and four off rates for ligand, three forward and three back allosteric transition rates for the doubly-liganded forms, and three transition state positional parameters) necessary to define the $B_i \rightleftharpoons A_i$, $A_i \rightleftharpoons I_i$, and $I_i \rightleftharpoons D_i$ allosteric transitions with two equivalent agonist binding sites per molecule, parameter values were deduced for the acetylcholine receptor on the basis of results with rapid agonist application techniques using outside-out patches containing embryonic-like nicotinic acetylcholine receptor from mouse muscle (Franke et al. 1993) and earlier single-channel measurement (Colquhoun and Sakmann 1985). Although independent parameters are presented here exclusively in terms of rate constants, it should be noted that in many cases equilibrium relations may be used to ascertain values, as reflected for example in the linkage relationships concerning off rates: ${}^{A}k_{off} = ({}^{B}k_{off}\ {}^{A}k_{on}\ {}^{BA}c)/{}^{B}k_{on}$; ${}^{I}k_{off} = ({}^{A}k_{off}\ {}^{I}k_{on}\ {}^{AI}c)/{}^{A}k_{on}$; and ${}^{D}k_{off} = ({}^{I}k_{off}\ {}^{D}k_{on}\ {}^{ID}c)/{}^{I}k_{on}$. Following Franke et al. (1993), on rates are set near the diffusion limit at $1.5 \times 10^{8}\ s^{-1}$, with the value of ${}^{B}k_{off}$ set at $8000\ s^{-1}$ (Colquhoun and Sakmann 1985). The ratio establishes ${}^{B}K_{d}$ and a lower limit of ${}^{BA}c$ is set by the cooperativity of dose-responses to about 0.001, thereby defining ${}^{A}K_{d}$ and (with the assumption that ${}^{A}k_{on}$ remains near the diffusion limit) ${}^{A}k_{off}$. The values of ${}^{AB}k_{2}$ and ${}^{BA}k_{2}$ are set by the parameters α and β, respectively, from single-channel measurements (Colquhoun and Sakmann 1985) and define ${}^{BA}L_{2}$, with ${}^{BA}L_{1}$ and ${}^{BA}L_{0}$ increasing for each step of ligand removal by $1/{}^{BA}c$. The affinity of the I state can be estimated from the data of Franke et al. (1993, presented in their figure 13). Termination of channel opening results in a reduction of channel current to about 4% of the maximum value, with a time course corresponding to a value of ${}^{AI}k_{2} = 20\ s^{-1}$. This reduction indicates a value of ${}^{AI}L_{2} = 0.04$. Recovery following a 200 ms pulse of 0.1 mM acetylcholine occurs with a characteristic rate of $\sim 4\ s^{-1}$ (Franke et al. 1993), thereby defining the rate-limiting step on the recovery pathway, $I_2 \rightarrow I_1 \rightarrow I_0 \rightarrow A_0 \rightarrow B_0$. Since the dissociation of agonist from the I state cannot be slower than the overall recovery rate, an upper limit of ${}^{I}k_{off} = 4\ s^{-1}$ may be assigned. Assuming that ${}^{I}k_{on}$ is also near the diffusion limit, a value of ${}^{I}K_{d} = 2.7 \times 10^{-8}$ M is predicted. A value of $D_0 \sim 1\%$ was used, in order to correspond to the kinetic measurements (Franke et al. 1993) in which the $I \rightleftharpoons D$ transition was characterized experimentally on the basis of the slow diminution of steady-state current levels (from 4% to 0.1%) when agonist is applied for many minutes. This additional slow desensitization fixes an upper limit of ${}^{ID}L_{2} = {}^{DI}k_{2}/{}^{ID}k_{2} = 0.025$ and ${}^{ID}k_{2} = 0.05\ s^{-1}$ was set to give a minimum estimate for the slow time course in the absence of more extensive data. Since no information is provided in these data on D-state affinity, it is set to the same value as the I state, resulting in ${}^{DI}k_{2} = 0.0012\ s^{-1}$. Concerning the transition state positional parameter for the $A_i \rightleftharpoons I_i$ interconversions, data for the rate of recovery following a desensitizing pulse (Franke et al. 1993) require a value of ${}^{AI}p$ close to 1.0 in order to achieve a value of ${}^{IA}k_{0}$ sufficiently high so as not to limit recovery from desensitization to a rate below $4\ s^{-1}$. Similarly, a value of ${}^{ID}p$ close to 1.0 is adopted in order to maximize ${}^{DI}k_{0}$, since the consequence of a highly stabilized D state (Figs. 3, 4) is to predict low $D \rightarrow I$ rates and hence very long recovery times. Concerning the $B_i \rightleftharpoons A_i$, interconversions, the observations concerning brief open forms attributed to singly-liganded molecule (Colquhoun and Sakmann 1985) suggest much larger changes in β than in α, corresponding to a value of ${}^{BA}p \sim 0.2$. Single-channel simulations for the complete 12-state model were satisfactory with a value of ${}^{BA}p = 0.2$ and correspond to a fraction of A_0 molecules during recovery (Figs. 4c) of 0.0003. The fraction of A_0 falls progressively to 5×10^{-6} as ${}^{BA}p$ rises to 0.5. Therefore, future experiments to define the fraction of A_0 during recovery and the properties of singly-liganded molecules should permit the value ${}^{BA}p$ to be established more precisely

the macroscopic and molecular approaches is presented in the following section (see Fig. 7 below). The simulation programs are incorporated in an extensive computational and graphical environment that runs under UNIX; an equivalent version designated STOIC (Simulations of Transient Openings in Ionotropic-receptor Channels) within the MATLAB environment, suitable for PC or MAC, is available upon request or via the Internet (http://www.unige.ch:80/sciences/biochimie/Edelstein/Edelstein.html).

5 Properties

The microscopic and macroscopic descriptions are equivalent, when ensemble averages of stochastic simulations

for the former are used to generate the latter (Frenkel 1993). Moreover, single-channel measurements provide advantages in terms of the resolution of kinetic processes compared with macroscopic measurements. Therefore, one approach would be to assign the values of all independent kinetic parameters (Table 1) on the basis of data at the microscopic level, and proceed to a macroscopic description on the basis of ensemble properties and calculations of equilibrium constants from kinetic constants (Figs. 1, 2). However, certain critical features of the system, such as cooperativity in agonist binding, are for practical reasons more readily established in macroscopic measurements of the dose-response type. Although difficulties can arise from using an equilibrium-based analysis for a kinetic process (see Fig. 8), the observed cooperativity provides a minimum estimate of the Hill coefficient that serves to constrain the range of values of key equilibrium constants such as ${}^{BA}L_0$ and ${}^{BA}c$. These constants have repercussions through linkage relationships on many kinetic constants. Hence, in this section the information that may be extracted from the basic macroscopic data is considered first, in conjunction with certain rates (${}^{AB}k_2$, ${}^{BA}k_2$, ${}^{B}k_{off}$) obtained using single channels. Simulations at the single molecule level then follow and, finally, the relationship between the microscopic and macroscopic is fully evaluated.

5.1 Activation and the affinity of the open state (A) deduced with the allosteric model: comparison with the standard model

The cooperative activation of the receptor involves the $B_i \rightleftharpoons A_i$ transitions and is governed according to the allosteric formulation by the basic parameters, ${}^{BA}L_0$ and ${}^{BA}c$ (Fig. 2a). To achieve the observed levels of cooperativity for agonist binding observed in dose-response curves, with values of $n_{H,A} \sim 1.8$ [see (A8) in the Appendix], the value of ${}^{BA}c$ must be sufficiently low, $\sim 10^{-3}$. For example, with a value of ${}^{BA}c = 10^{-2}$, the average value of $n_{H,A}$ falls below 1.5 for all values of ${}^{BA}L_0$. Moreover, if the value of ${}^{BA}L_0$ were to lie outside the optimal range for cooperativity of agonist binding at two sites, ${}^{BA}L_0 \sim ({}^{BA}c)^{-1}$, even lower values of ${}^{BA}c$ would be required to achieve values of $n_{H,A} \sim 1.8$. However, if the value of ${}^{BA}c$ were too low, unrealistically high affinities for the A, I and D states would be required, given other limits described below. Possible anomalies in the estimates of cooperativity derived from using the dose-response analysis (based on an equilibrium model) for channel activation (a kinetic process) are evaluated in Sect. 6.

The value of ${}^{BA}L_0$ is further restricted by the data for closing and opening rates (α and β, respectively) observed in single-channel measurements. These constants characterize the $B_2 \rightleftharpoons A_2$ transitions, with the $B_2 \rightarrow A_2$ rate set by $\beta = {}^{BA}k_2 = 30\,000\ s^{-1}$ and the $A_2 \rightarrow B_2$ rate set by $\alpha = {}^{AB}k_2 = 700\ s^{-1}$ (Colquhoun and Sakmann 1985). These values of α and β are in general agreement with those in other investigations based on single-channel measurements (Lingle et al. 1992) or experiments with photoactivation of agonist (Matsubara et al. 1992). Since linkage relationships developed in Fig. 2a require that ${}^{BA}L_2 = {}^{AB}k_2/{}^{BA}k_2$, the ratio of α/β yields a value of ${}^{BA}L_2 = 0.023$. Moreover, since ${}^{BA}L_2 = {}^{BA}L_0\ ({}^{BA}c)^2$, for a value of ${}^{BA}c \sim 10^{-3}$, a minimum value of ${}^{BA}L_0 \sim 2 \times 10^4$ is required, which is sufficiently high to reflect the low degree of spontaneous channel opening in the absence of ligand (Jackson 1986).

To relate the affinity ratio, ${}^{BA}c$, to absolute values, it is necessary to establish the strength of agonist binding. The available evidence indicates a very rapid rate of agonist binding, with the value of ${}^{B}k_{on} = 1.5 \times 10^8\ M^{-1}\ s^{-1}$ assigned by Franke et al. (1993). Single-channel measurements have also established the off rate for the B state at ${}^{B}k_{off} = 8000\ s^{-1}$ (Colquhoun and Sakmann 1985). Hence the affinity of the B state is fixed by the ratio of the kinetic constants, ${}^{B}K_d = {}^{B}k_{off}/{}^{B}k_{on} = 53\ \mu M$. With the value of ${}^{BA}c = 1.08 \times 10^{-3}$, the affinity of the A state corresponds to ${}^{A}K_d = 57\ nM$ (Table 1). Assuming that the rate of agonist binding to the A state is the same as for binding to the B state (as is likely since the affinity of A is stronger, but the on rate is already near the diffusion limit), ${}^{A}k_{on} = 1.5 \times 10^8\ M^{-1}\ s^{-1}$ and a value of ${}^{A}k_{off} = 8.6\ s^{-1}$ is required to satisfy the value of ${}^{A}K_d = 57\ nM$.

The affinity of the A state deduced in this way differs considerably from the generally accepted value obtained according to the standard model (Colquhoun and Sakmann 1985), which assimilates channel opening to the doubly-liganded molecules (or in some cases to singly-liganded molecules) but without indicating the origin of the energy responsible for channel opening, according to the sequence:

$$B_0 + 2X \overset{{}^{B}K_d}{\rightleftharpoons} B_1 + X \overset{{}^{B}K_d}{\rightleftharpoons} B_2 \underset{\alpha}{\overset{\beta}{\rightleftharpoons}} A_2 \qquad (1)$$

This formulation implies an apparent affinity for the A state reflected by ${}^{App}K_d = EC_{50}$, where ${}^{App}K_d = {}^{B}K_d\ (\alpha/\beta)^{1/2} = 8\ \mu M$ (for ${}^{B}K_d = 53\ \mu M$, $\alpha = 700\ s^{-1}$, and $\beta = 30\,000\ s^{-1}$). In contrast, the allosteric formulation reveals that there is a substantial 'hidden' energy for the tight binding to the A state (${}^{A}K_d = 57\ nM$) that is required to overcome the intrinsic stability of the closed B state.

5.2 Desensitization and the kinetic pathway selected for recovery

Following activation governed by the parameters for the B and A states described above, receptors undergo spontaneous transitions to the desensitized states, I and D, in the time range of 0.1–100 s (Changeux 1990). The transitions between states may be visualized in the kinetic simulation presented in Fig. 4 with values of the parameters in Table 1. Because the data occur over several time regimes, the ligand-gated response (Fig. 4a) and the evolution of the various states (Fig. 4b) are presented as a function of time on a logarithmic scale. Since the concentration of agonist is high, this simulation follows the path $B_0 \rightarrow B_1 \rightarrow B_2 \rightarrow A_2 \rightarrow I_2 \rightarrow D_2$. At early times the progression from unliganded to liganded forms

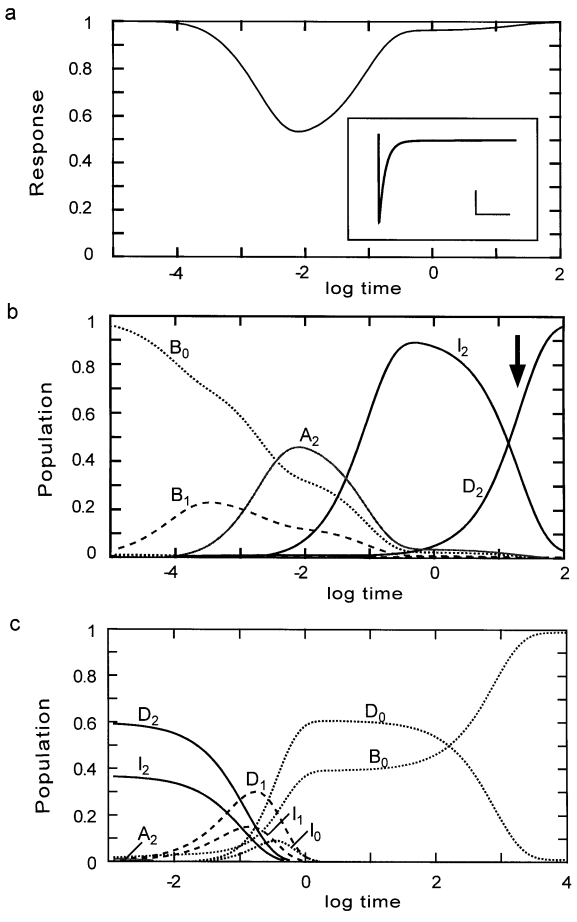

Fig. 4a–c. Kinetic simulation presenting activation, progression through the states upon agonist binding, and recovery following agonist removal. The states are labelled, with the number of ligand molecules bound indicated by the line format (0, *dotted*; 1, *dashed*; 2, *continuous*). The ligand concentration is 10^{-5} M. Values of the parameters utilized are presented in Table 1. **a** The appearance of the open state (in the form of a current change, 1 − [A states]) on a scale of log time (in seconds), with the *inset* presenting the same data on a linear scale (vertical bar = 0.1 fractional amplitude change; horizontal bar = 0.5 s). **b** The fractional population represented by each of the four states in the time range 10^{-8} to 10^{2} s during an agonist pulse, on a logarithmic scale **c** Recovery begins upon removal of free agonist at the point marked by the arrow in **b**, corresponding to an agonist pulse of 20 s

is apparent for B, followed by interconversion of biliganded B to biliganded A and I. Transient channel opening corresponds to the appearance and disappearance of A. The population of biliganded D increases only at longer times via conversion from biliganded I due to the slow rate of the $I_2 \rightarrow D_2$ interconversion.

A kinetic simulation of recovery based on the values in Table 1 is presented in Fig. 4c, demonstrating that with ${}^{AB}k_0 \gg {}^{IA}k_0$, recovery along the pathway: $I_0 \rightarrow A_0 \rightarrow B_0$ occurs with a passage through the A_0 state so rapid that channel opening is negligible. Following agonist removal, the I_2 state loses agonist molecules and is rapidly transformed to B_0 in less than 1 s. The D_2 state loses agonist molecules to form D_0 within 10 s, but requires long times (10^3–10^4 s) to re-equilibrate with B_0 to return to the initial low levels. Such long recovery times could account for certain slow physiological responses (see Discussion). Overall, it is clear from this simulation that the four-state model predicts virtually negligible channel opening during the recovery period, but without the necessity of invoking a distinct cyclic pathway from I (or D) to B without passage through A, as required in the standard cyclic model (Katz and Thesleff 1957; Colquhoun and Sakmann 1985; Franke et al. 1993).

5.3 Simulations of single channel events and reconstruction of macroscopic processes

A satisfactory kinetic model must be able to represent both single-channel and macroscopic events. The way in which the two descriptions of the system may be related is presented in this section. The properties of the model in response to agonist binding are described initially in terms of the single-channel events predicted for a receptor molecule with zero, one, or two agonist molecules bound, as presented in Fig. 5a, b and c, respectively. In the time range of the simulations, transitions to the D_i states are highly improbable and hence were not included in this example, but are restored for complete simulation (see Fig. 6). For unliganded forms channel opening is a rare event, with a few brief openings observed in the 2 s simulation (Fig. 5a). When one agonist is bound per molecule of receptor, longer and much more frequent channel opening is predicted (Fig. 5b). When two agonists are bound the behaviour, as represented in Fig. 5c, corresponds to the characteristic bursts of channel opening (Sakmann et al. 1980), with brief closures during the bursts indicating returns from A_2 to B_2 and long quiescent periods of passage to the desensitized state I_2. Passage from A_2 to I_2 is less probable than passage to B_2 (because ${}^{AI}k_2 \ll {}^{AB}k_2$), but once the I_2 state is reached, the low value of ${}^{IA}k_2$ results in a relatively long time on average until a return to A_2 is achieved.

The single-channel simulations involving all four states at all possible degrees of ligand binding provide a complete description of the system, as presented in Fig. 6 for a sampling of the predicted behaviour at several ligand concentrations. Recordings of the ensemble of the states permit each channel opening/closing event to be resolved into the underlying transition between conformational states. For the series of three agonist concentrations presented, there is a clear transition from occasional openings at 10^{-6} M (Fig. 6a), to sustained bursts with brief closures at 10^{-4} M (Fig. 6c), with intermediate behaviour at 10^{-5} M (Fig. 6b). At high concentrations of agonist, the characteristic bursts with brief closures involve transitions mainly from A_2 to B_2, but occasionally to B_1 and B_0 as well (Fig. 6c). In longer simulations (data not shown), at 10^{-3} M, sustained passage occurs through the D states (exclusively D_2 and D_1).

While the stochastic properties represented by individual single-channel simulations (Fig. 6a–c) are coherent with respect to the formulations of the model and the general properties of the system, a rigorous test involves the demonstration that the average properties of a large number of individual single-molecular channel simulations agree with the overall (macroscopic) properties

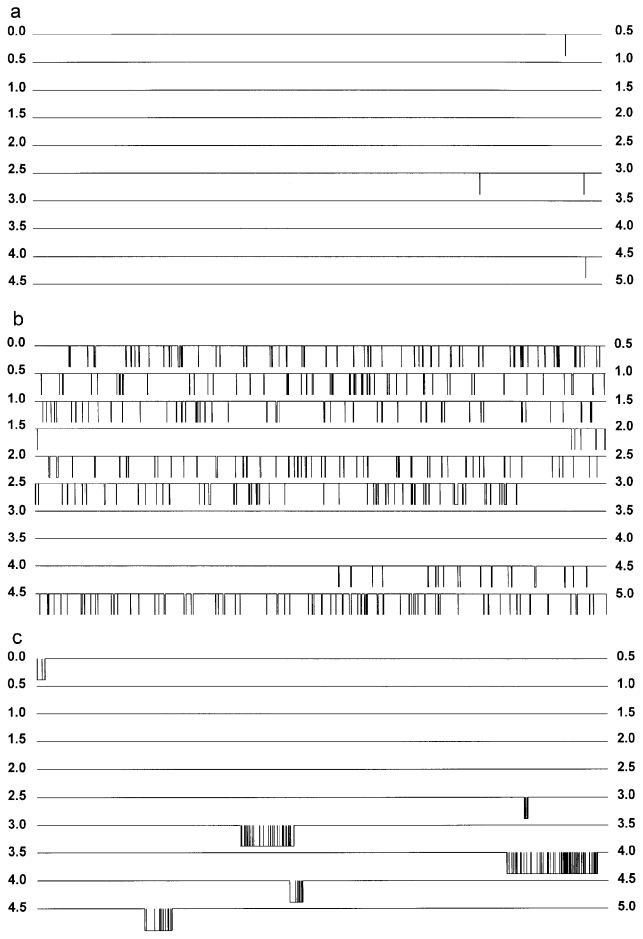

Fig. 5a–c. Single-channel simulations for unliganded and mono- and biliganded receptors. The three panels describe the transitions for single molecules between the states (with opening indicated by a downward displacement of the simulated trace), as a function of time (in seconds). **a** $B_0 \rightleftharpoons A_0 \rightleftharpoons I_0$. **b** $B_1 \rightleftharpoons A_1 \rightleftharpoons I_1$. **c** $B_2 \rightleftharpoons A_2 \rightleftharpoons I_2$. The simulations were performed with standard matrices with the parameters of Table 1 on the basis of the following principles. For the stochastic evolution of a single receptor channel, the method of Gillespie was employed (Steinfeld et al. 1989; Korn and Horn 1991). For example, as applied to the transitions of the doubly-liganded forms (**c**), the system is characterized by the four kinetic constants defined by the reactions:

$$B_2 \underset{{}^{AB}k_2}{\overset{{}^{BA}k_2}{\rightleftarrows}} A_2 \underset{{}^{IA}k_2}{\overset{{}^{AI}k_2}{\rightleftarrows}} I_2$$

The Gillespie algorithm is based on a reaction probability density function, $P(\tau, i)$, where $P(\tau, i)\,d\tau$ is the probability at time t that an R_i transition between states will occur in the differential time interval $(t+\tau,\ t+\tau+d\tau)$. The probability $P(\tau, i)$ can be expressed as the product of the probability of a reaction occurring in time interval $d\tau$ and the probability of that reaction being an R_i transition between states: $P(\tau, i) = P(\tau) \cdot P(i)$. The function $P(\tau)$ is known as an exponential random variable with parameter a, such that $\tau = (1/a)\ln(1/r_1)$, where a is calculated by summing all the rates for leaving the current state, i.e. ${}^{AB}k_2 + {}^{AI}k_2$ for the A_2 state, and r_1 is a uniform random number between 0 and 1 (Press et al. 1986). The function $P(i)$, based on a second uniform random number between 0 and 1, r_2, is used to choose the direction of the next transition, in conjunction with a T matrix:

$$\mathbf{T} = \begin{bmatrix} 0 & {}^{AB}k_2/({}^{AB}k_2 + {}^{AI}k_2) & 0 \\ {}^{BA}k_2/{}^{BA}k_2 & 0 & {}^{IA}k_2/{}^{IA}k_2 \\ 0 & {}^{AI}k_2/({}^{AB}k_2 + {}^{AI}k_2) & 0 \end{bmatrix}$$

The T matrix is used for dividing the interval between 0 and 1 into regions proportional to the probability of the reaction direction. In the case of the receptor in the A_2 state, the second column of the T matrix, $[0.99886, 0, 0.00114]^T$, defines two regions, [0, 0.99886] and [0.99886, 1], that determine whether the next transition is to B_2 or I_2. For example for $r_2 = 0.99997$, the transition is to I_2, whereas for $r_2 = 0.69410$, the transition is to B_2. Using a similar approach, the transition probabilities were calculated for the non-liganded and mono-liganded forms. In addition, by extending the analysis to all 12 states (B, A, I, and D, with 0, 1, or 2 agonists bound), the full time-dependence and ligand-dependence were computed, as presented in Fig. 6. The rates of the transitions were deduced on the basis of the published data for the biliganded forms and the estimates of the transition state positional parameters (Fig. 2b) to obtain the values of the other forms, as described in the legend to Fig. 6

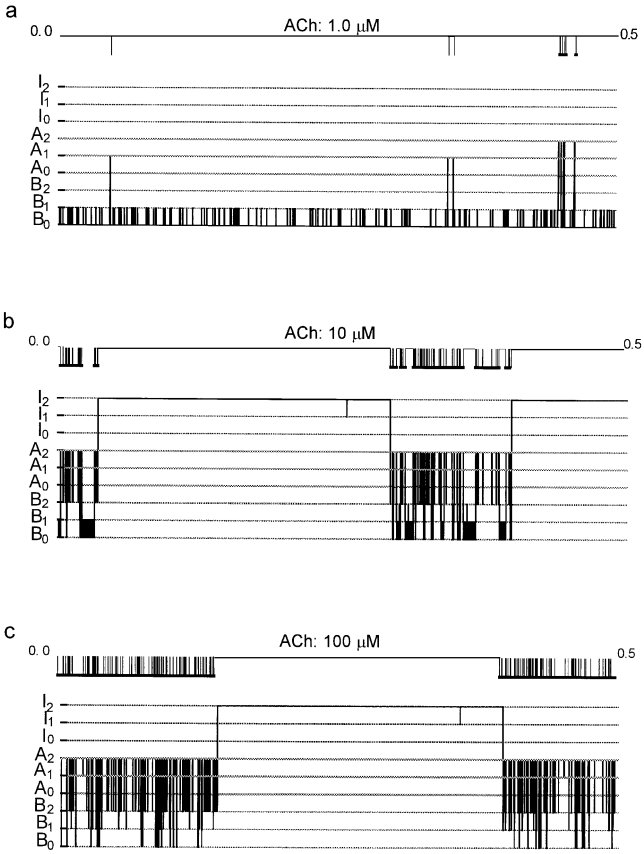

Fig. 6a–c. Predicted behaviour of single channels as a function of ligand concentration and the relation to macroscopic properties. The simulations described separately in Fig. 5 for each degree of ligand binding were expanded to all 12 states (B_i, A_i, I_i, and D_i, for i = 0, 1, and 2) and a defined concentration of agonist: **a** 10^{-6} M; **b** 10^{-5} M; **c** 10^{-4} M. For each panel the simulation of channel opening/closing events during 0.5 s are at the *top* (with opening indicated by a downward displacement of the simulated trace). The nature of the event in terms of the transitions among the nine states involved (no transitions to D states were observed for the conditions presented) are depicted below each event. Passages through A_0, A_1, or A_2 are defined as the open state of the channel. Values of the parameters from Table 1 were used. Other details are as described in the legend to Fig. 5

observed with the standard kinetic analysis (Fig. 4). Tests along these lines were constructed by summing the properties observed in simulations with 8, 16, 32 or 64 independent receptors. As the number of receptors is increased, the signal/noise ratio of the ensemble increases.

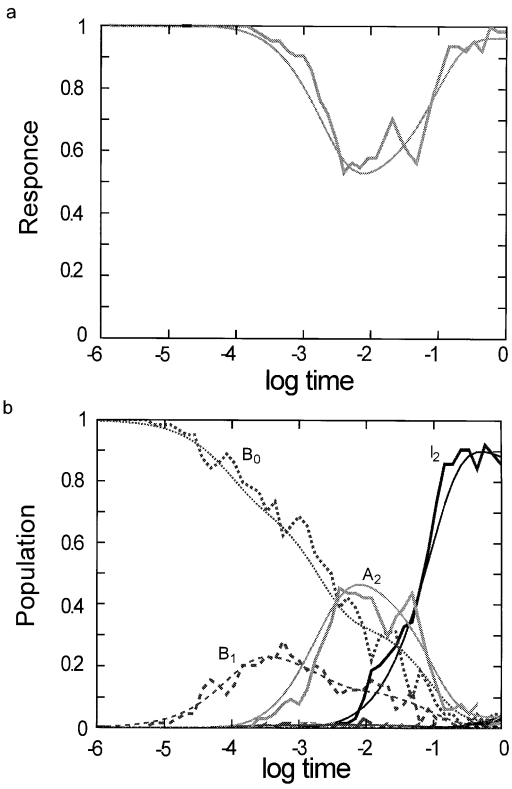

Fig. 7. The comparison of the composite of 64 single-channel simulations at an agonist concentration of 10^{-5} M and the macroscopic properties of a standard kinetic simulation, as presented in Fig. 4 for **a** the channel opening curve (1 − [A states]) and **b** the fractional populations versus log time (in seconds). The average data for the 64 channels are presented with the *thicker lines* for the states as in Fig. 4, with the exception that the D state is not presented

With 64 receptors, although the noise level is still significant, the composite properties closely resemble those obtained in the complete kinetic simulation corresponding to an unlimited number of receptors. The agreement can be observed for the simulated dose-response curve in Fig. 7a and the amplitudes of the individual states in Fig. 7b.

6 Applications

6.1 Kinetic simulations of dose-response curves to test EC_{50} determinations

The dose-response analysis has been widely used for characterization of the cooperativity and affinity (EC_{50}) of ligand-gated channels, but it is important to ascertain under what conditions such an equilibrium-based analysis is appropriate for a transient phenomenon. Therefore, simulations were performed with the complete four-state model to test this issue. Although the rate constant for agonist binding is very fast, approaching the diffusion limit, at the relevant agonist concentrations for activation, 10^{-6} to 10^{-3} M, the effective times of activation are limited by the arrival of agonist to the range 0.01–10 ms. These times are close to the speed of the initial phase of

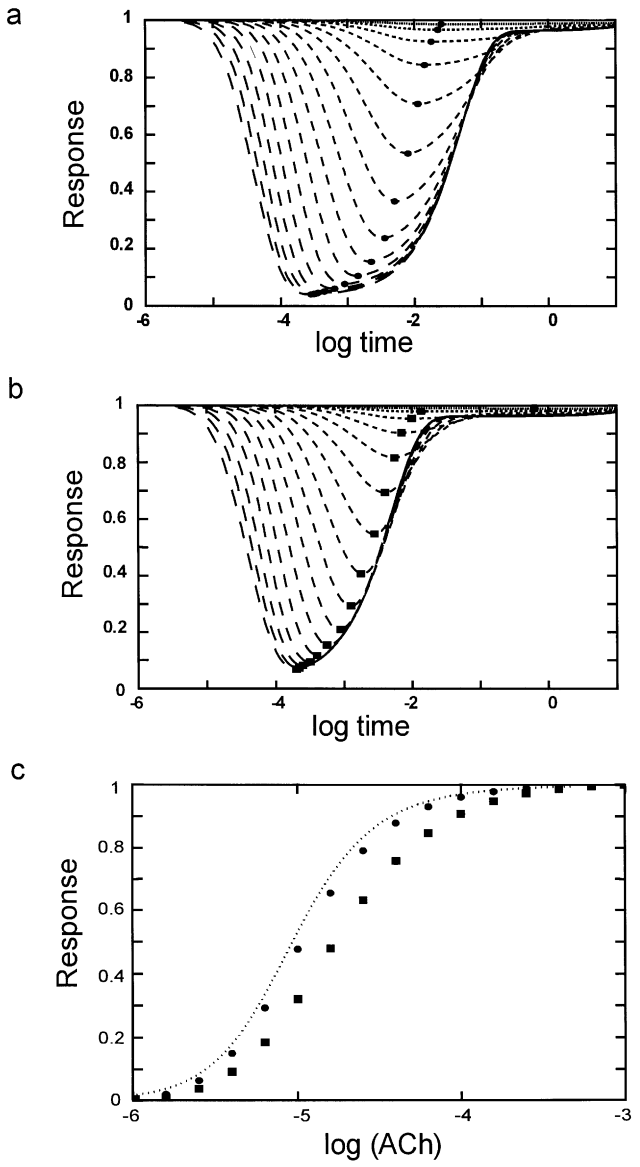

Fig. 8a–c. Dose-response simulations. **a** Kinetic simulations for increasing concentrations of agonist in the concentration range 10^{-6} to 10^{-3} M, with the value of $^{AI}k_2 = 20\ s^{-1}$deduced for the acetylcholine receptor (Table 1). Simulations for each concentration (in increments of $10^{0.2} = 1.58$ times the previous concentration) are presented as $1 - \bar{A}_{norm}$ versus log time (in seconds) and the minimum of each curve, corresponding to the maximal channel opening at that concentration, is marked by a *filled circle*. **b** Kinetic simulation as in **a**, but with a test value of $^{AI}k_2 = 200\ s^{-1}$ and with the maximal channel opening at each concentration marked by a *filled square*. **c** Dose-response curves for the simulation in **a** and **b**. The predicted curve derived from the theoretical equilibrium (A6) with the parameters of Table 1 is presented as the continuous *dotted line*; the individual points for maximal channel opening at each concentration from **a** and **b** are transferred to give the corresponding filled circles and filled squares, respectively

desensitization, with the $A_2 \rightarrow I_2$ transition characterized by the rate constant $^{AI}k_2 = 20\ s^{-1}$ (Table 1), resulting in systematic errors in the apparent values of the Hill coefficient, n_H, and EC_{50}, as described in Fig. 8. The errors are relatively minor for the value of $^{AI}k_2 = 20\ s^{-1}$

(Fig. 8a, c), but by comparing the full dose-response curve at higher and lower values of $^{AI}k_2$, it is clear that distortions are inherent in the dose-response analysis. For example, the apparent values of the Hill coefficient and affinity at $^{AI}k_2 = 20\,s^{-1}$, $n_H = 1.6$ and $EC_{50} = 10\,\mu M$, differ only slightly from the values observed with a desensitization sufficiently low ($^{AI}k_2 = 2\,s^{-1}$) to avoid any distortions: $n_H = 1.7$ and $EC_{50} = 9\,\mu M$. Hence, for both the n_H and EC_{50} values, the constellation of rate constants for the AChR (Table 1) is such that errors are limited to $\sim 10\%$ (Fig. 8c). However, were the $^{AI}k_2$ value 10-fold faster ($^{AI}k_2 = 200\,s^{-1}$), the relevant values would be $n_H = 1.3$ and $EC_{50} = 20\,\mu M$ (Fig. 8b, c), with major discrepancies between the apparent and true (desensitization-free) properties. If the desensitization rate were further accelerated to $^{AI}k_2 = 2000\,s^{-1}$, the apparent values would be distorted to $n_H = 1.24$ and $EC_{50} = 50\,\mu M$ (data not shown).

6.2 Kinetic simulations of desensitization with low-concentration pre-pulses to test IC_{50} determinations

An important feature of ligand-gated channels is the desensitization by low concentrations of agonist that are insufficient to provoke significant channel opening but reveal desensitization when followed by a stronger pulse (Katz and Thesleff 1957; see also Rang and Ritter 1970). By studying a range of pre-pulse concentrations and plotting the fraction of residual activity observed with the strong pulse, desensitization curves are obtained with the mid-point defining an apparent inactivation constant, IC_{50}. Typically, the pre-pulse is applied for a duration of ~ 10 s (Franke et al. 1993). If equilibrium conditions prevailed, the IC_{50} value obtained would be related to the dissociation constant for the high-affinity sites of the desensitized state (Heidmann and Changeux 1978). Therefore, to test whether the equilibrium assumption is reasonable for such an analysis, simulations were performed at very low concentrations of ligand. As presented in Fig. 9, kinetic simulations reveal that for a low concentration such as 0.4 μM, progression through the B-A-I-D states is relatively slow and for a 10-s pre-pulse some I state appears, but only a small fraction of the D state that would be produced by a pulse sufficiently long (~ 1000 s) to reach the final equilibrium value. The initial events are more readily visualized on a logarithmic scale (Fig. 9a), with the slower events depicted on a linear scale (Fig. 9b). When a series of simulations at different concentrations are performed, the degree of desensitization after 10 s can be measured and compared with the equilibrium value of desensitization. In this way a hypothetical curve for the determination of IC_{50} is produced for the equilibrium properties and compared with the simulated values with 10-s pre-pulses. These data, presented in Fig. 9c, show the systematic divergence of the two curves. The points obtained from the simulations for 10-s pre-pulses are considerably to the right of the equilibrium curve, and would imply an apparent affinity for the D state using IC_{50} values that is significantly weaker than the true equilibrium value.

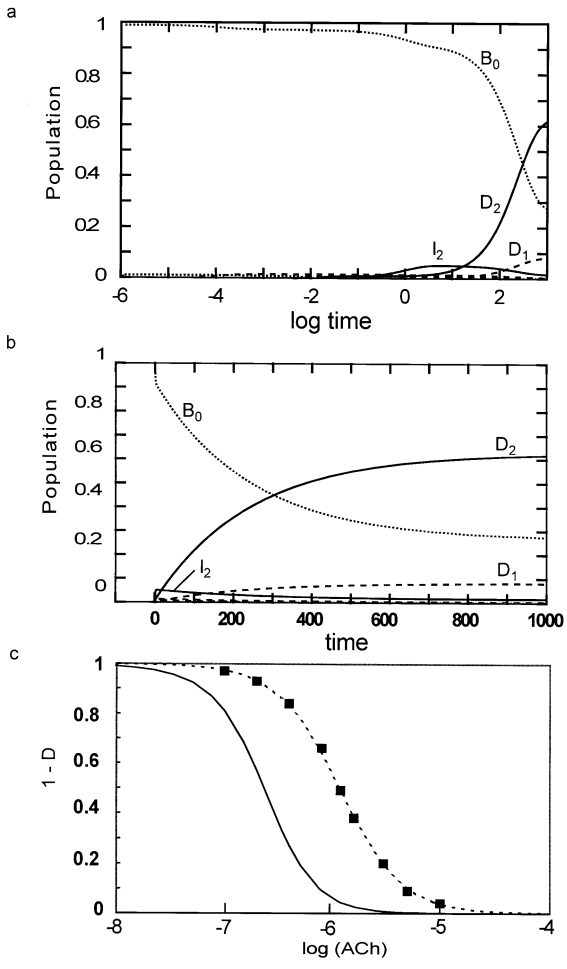

Fig. 9a–c. Simulations of pre-pulse desensitization with low concentrations of agonist. Simulation of the populations of states for an agonist concentration of 4×10^{-7} M, with data presented as a function of log time (**a**) or time in seconds (**b**); with the states as labeled. **c** Inhibition-response curve to obtain apparent IC_{50} values. Solid line predicted by the allosteric theory (equation A11) with an IC_{50} values of 2.66×10^{-7} M; points from a series of simulations as in (**a**) for the fraction of activatable receptors remaining after a 10 s prepulse at different concentrations of ACh. The dashed curve through the points corresponds to an apparent IC_{50} value of 1.2×10^{-6} M

6.3 Modulations by allosteric effectors and coincidence detection

Various modifications of the functional properties of the AChR are produced by non-covalent interactions with pharmacological agents and other modulators (Léna and Changeux 1993), and covalently by phosphorylation (Huganir and Greengard 1990; Levitan 1994). In general, when differences in current are observed in the presence and absence of a potential allosteric effector, it has not been determined whether affinity changes and/or specific conductance changes are responsible for the differences. In this respect the study by Mulle et al. (1992) is of particular interest, since potentiation by calcium was observed to coincide with an increase (approximately 3-fold) in the frequency of channel opening. A model of

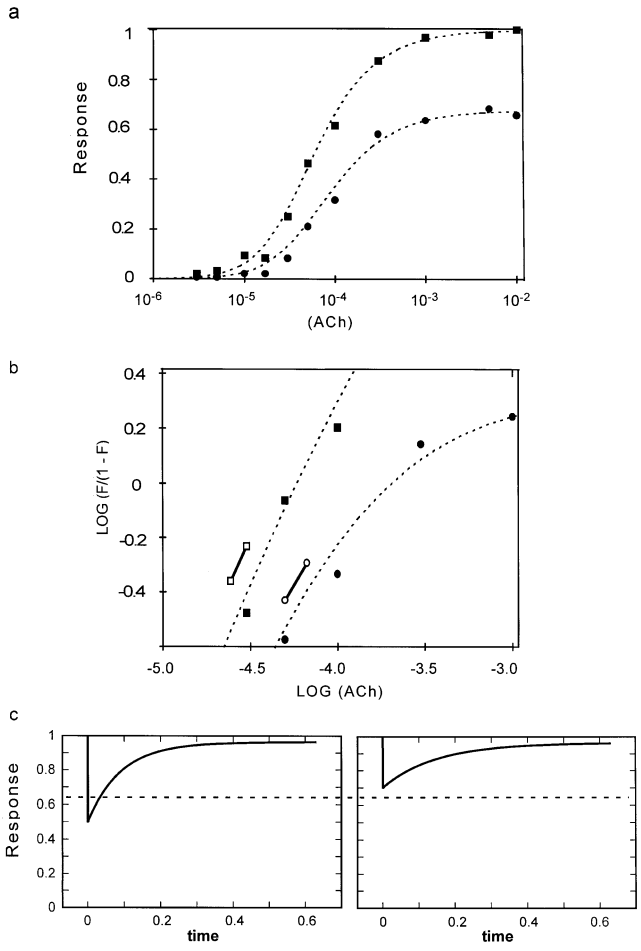

Fig. 10a–c. Data and theoretical curves for the potentiation of rat medial habenular neurons by external calcium. **a** Dose-response curves for the effect of acetylcholine and currents in the presence of 4 mM calcium (solid squares) and in the absence of added calcium (solid circles) from the report by Mulle et al. (1992). The dashed lines are obtained with the four-state allosteric model using the parameters of Table 1, with the exception of the values of ${}^{BA}L_0 = 5.25 \times 10^5$ for the curve on the left corresponding to the presence of 4 mM calcium and ${}^{BA}L_0 = 1.25 \times 10^6$ for the curve on the right corresponding to no added calcium. **b** Hill plots for the central portions of the data in **a**, with the short bars terminating with open squares or open circles corresponding to the slopes of the Hill equation of $n_H = 1.4$ and $n_H = 1.1$, respectively. (**c**) Illustration of coincidence detection. For kinetic simulations (time in seconds) with an agonist concentration of 2×10^{-4} M, only the response on the left with ${}^{BA}L_0 = 5.25 \times 10^5$ (corresponding to 4 mM calcium) and not the response on the right with ${}^{BA}L_0 = 1.25 \times 10^6$ corresponding to no calcium, reaches a hypothetical threshold for neuronal firing (dashed line)

these data presented in Fig. 10 indicates that the potentiation by calcium can be represented simply in terms of a 2.3-fold reduction in the allosteric constant, ${}^{BA}L_0$, with all other parameters remaining unchanged from the values in Table 1. The lower value of ${}^{BA}L_0$ is sufficient to account for the shift of the curve to the left, the augmented maximal response (Fig. 10a), and the increased cooperativity (Fig. 10b). The effect of calcium is thus a true allosteric modulation, since the change in frequency of opening indicates an altered ${}^{BA}k_2$ that corresponds closely to the change estimated for ${}^{BA}L_0$, since ${}^{BA}L_0 {}^{BA}c^2 = {}^{AB}k_2/{}^{BA}k_2$.

Allosteric effects of the type observed for potentiation by calcium have a number of implications for regulation of activity in the nervous system. At synapses, allosteric modulators could provide coincidence detection (Changeux and Heidmann 1987). Such an effect for acetylcholine (ACh) and calcium may be visualized in Fig. 10c, assuming a constant threshold that is attained only in the presence of both ACh and calcium (on the left), but not with ACh alone (on the right). Since calcium may enter neurons via the open ligand-gated cation channel of various neuronal AChR or voltage-gated channels, regulatory effects may also be produced related to intracellular accumulation (such as phosphorylation) or extracellular depletion (such as habituation resulting from repeated stimulation by ACh). In addition to its role in regulating synaptic efficiency, diminished extracellular calcium concentrations could also participate in retrograde signalling.

Similar effects involving a right-shifted dose-response curve with a diminished maximal response amplitude are observed for modulators such as steroids (Valera et al. 1992). Allosteric effects may also involve modulation of desensitized states, as for example is observed with substance P (Valenta et al. 1993) or following phosphorylation with cAMP-dependent protein kinase (Huganir et al. 1986). Overall, any substance that alters the pre-existing equilibria between states can exert an effect on synaptic efficiency (Changeux 1990).

7 Discussion

The allosteric model with pre-existing equilibria between a minimum of four conformation states, B, A, I and D, satisfactorily accounts for the kinetic properties of the AChR in vivo and in vitro. Application of the model to single-channel events by conversion of kinetic constants into probabilities of microscopic events clarifies the effects of ligand binding on the patterns of interconversions between the various states, particularly the nature of the bursts typical of single channels at moderately high concentrations of agonist (Fig. 6). The formulation of the model in terms of single-channel events also opens the possibility for simulations at the level of a synapse, with a finite number (approximately 10^3) of receptors. While many issues remain to be clarified in order to model a synapse more accurately, particularly with respect to quantal analysis (Bekkers 1994), simulations with a fully functional model of the type presented here could provide new insights, since previous efforts have not included desensitization (Bartol et al. 1991; Faber et al. 1992). With respect to artificial neural networks, an understanding of these aspects should lead to more realistic modelling. While synaptogenesis has also been considered and incorporated in some models (Foldiak 1990; Adelsberger-Mangan and Levy 1994), detailed schema based on experimental observation have been proposed mainly for the neuromuscular junctions (Gouzé et al.

1983). Other important features for the development of more biologically realistic modelling concern delays and oscillatory behaviour (Herz et al. 1989; Kerszberg and Zippelius 1990; Buonomano and Merzenich 1995; Hopfield 1995; Kerszberg and Masson 1995; Hangartner and Cull 1996), but these aspects have not as yet been brought to the molecular level with respect to ligand-gated ion channels and metabotropic receptors. In contrast, for the basic concept of synaptic plasticity (Hebb, 1949), as applied in numerous models (Bienenstock et al. 1982; Amit, 1989; Churchland and Sejnowski 1992; Edelman et al. 1992; Montague and Sejnowski 1994), plausible mechanisms based on allosteric regulation of ligand-gated channels have been formulated, particularly in relation to synaptic triads (Heidmann and Changeux 1982; Dehaene et al. 1987; Changeux and Dehaene 1989; Changeux 1993). In this approach, signals produced by a synaptic terminal C acting on neuron B are assumed to regulate the efficacy of the post-synaptic synapse of $A \rightarrow B$ with an allosteric switch of postsynaptic receptors from neuron B. Applications of the model have proved to be fruitful in the formalization of neural networks able to perform a number of complex tasks, such as the Wisconsin card sorting test (Dehaene and Changeux 1991). The regulatory effects could intervene to stabilize one of the allosteric conformations and as a consequence alter the corresponding rates of interconversion. Another feature of neural networks that has received considerable attention is the issue of coincidence detection (Montague and Sejnowski 1994). While the NMDA receptor is generally considered the main ligand-gated receptor responsible for coincidence detection on the basis of its voltage dependent Mg^{2+} channel block (Wigstrom and Gustafsson 1985), we have suggested that allosteric effectors operating at sites distinct from the channel can also produce coincidence detection (Fig. 10).

With respect to other features of ligand-gating of the AChR, several new concepts emerge. (1) Activation results from the $B_i \rightleftharpoons A_i$ equilibrium, but requires a high affinity of the A state, some 140-fold stronger than previous estimates (Colquhoun and Sakmann 1985; Franke et al. 1993). (2) Cooperativity of the ACh dose-response curve arises from the $B \rightarrow A$ allosteric transition, but without limiting channel opening only to receptors with two molecules of ligand bound, as in the phenomenological scheme (Katz and Thesleff 1957; Colquhoun and Sakmann 1985; Franke et al. 1993). (3) Recovery from desensitizing pulses with minimal channel opening appears as a consequence of the energy barriers (Fig. 3) that permit rapid passage through the A_0 state along the sequence $I_0 \rightarrow A_0 \rightarrow B_0$ (Fig. 4b), without the necessity of invoking a separate cyclic pathway, as required in the standard model (Franke et al. 1993). (4) The conventional dose-response analysis is shown to be a hazardous approximation due to the application of an equilibrium theory to a complex kinetic process involving both activation and desensitization, although only relatively limited distortions are produced for the AChR due to a sufficiently slow desensitization rate (Fig. 8). (5) The utilization of the low-concentration pre-pulse method to evaluate desensitization is shown to produce measurements of IC_{50} that introduce systematic distortions, since the system is far from equilibrium unless pre-pulse duration times approach tens of minutes (Fig. 10).

Because of these latter limitations for obtaining equilibrium IC_{50} values, considerable additional data would be required with long pre-pulse times in order to define the parameters of the D state more fully. Recovery times from the D state may be extremely long (hours), since they will be limited by ${}^{DI}k_0$, which may be as low $\sim 10^{-4}\ s^{-1}$ (Table 1; see also Fig. 4c). It is interesting to note that slow structural changes have been reported (Chang and Bock 1977). Response times in this range could contribute to upregulation, downregulation, and other pharmacological effects associated with both chronic and acute nicotine administration (Ochoa et al. 1990; Lukas and Bencherif 1992). Heavy and light smoking regimes may be related to maintaining the D state by the former, and permitting stimulatory effects via action on the A state by the latter (Wonnacott 1990).

The model developed here satisfactorily represents the functional data for the AChR in the various forms presented. However, alternative models may exists that represent the data well. With respect to the four-state allosteric model studied in this report the major competing alternatives fall into two categories. First, there is the more general tetrahedral model (Fig. 1d), for which the linear variant developed here (Fig. 1e) is formally a specific simplification. The equilibrium relationships between the four states are identical for the full tetrahedral model and the linear simplification, but the predictions for the kinetics of interconversions between states differ. Transitions follow the pathway $B \rightleftharpoons A \rightleftharpoons I \rightleftharpoons D$ in the linear scheme. The other interactions ($B \rightleftharpoons D$, $B \rightleftharpoons I$, or $A \rightleftharpoons D$) are assumed to be characterized by energy barriers sufficiently high to render these kinetic pathways negligible under the conditions of the cases examined here. For example, the $I \rightarrow D$ transition in the 10 s range compared with the $B \rightarrow A$ transition in the millisecond range (Table 1), implies that a direct $B \rightleftharpoons D$ pathway would be negligible, involving at most one molecule in 10^4 (if the $B \rightleftharpoons D$ barrier were no higher than the $I \rightleftharpoons D$ barrier). For a direct $B \rightleftharpoons I$ passage the relative barrier heights suggest at most one molecule in 10^3, and at most one molecule in 400 for a direct $A \rightleftharpoons D$ passage. In effect, among the possible pathways between states, the kinetic barriers lead to selection of a linear order in the progression between states (Fig. 1e). Within the linear scheme (Figs. 3, 4), a second level of pathway selection occurs for the distinct progression of activation ($B_2 \rightarrow A_2 \rightarrow I_2$) versus recovery ($I_0 \rightarrow A_0 \rightarrow B_0$).

The second category of competing models concerns those with fundamentally different initial assumptions, as for mechanisms of the sequential type (Koshland et al. 1966) which limit conformational states in the absence of ligand to the basal state. In this respect such models are not in accord with the observations of spontaneous channel opening (Jackson 1986). Stepwise models of the sequential type have been satisfactorily applied to receptors (Auerbach 1993), but were not confronted with the range of properties presented here. In principle, a sequential model could incorporate the conductance substates

reported for the AChR (Colquhoun and Sakmann 1985) more readily than an allosteric model with concerted transitions. However, the incidence of conductance substates is low, accounting for only about 1% of the events recorded by Colquhoun and Sakmann (1985) – less than would be expected for intermediate conformational states. In general, the sequential-type models require overlapping ligand-binding and conformational change functions, whereas these functions can diverge according to the allosteric formulation. This difference, which has served to distinguish between models for allosteric enzymes (Changeux and Rubin 1967; Schachman 1988), might also be exploited for ionotropic receptors, for example with fluorescent ligands that permit site occupancy and channel opening to be monitored independently, as suggested previously (Changeux and Edelstein 1994).

For the present investigation the two sites for agonist have been modelled exclusively with the assumption of an identical affinity. The justification for this assumption has been reviewed elsewhere (Changeux and Edelstein 1994), but for certain data sets it may be necessary to introduce non-equivalent agonist binding sites, particularly for the complexities arising from the hetero-oligomerization of the various combinations of neuronal AChR (Role 1992; Sargent 1993; Galzi and Changeux 1994). Dose-response curves with Hill coefficients approaching 5 suggest that up to five agonist sites appear to be required for $\alpha 7$ in certain cases (Bertrand et al. 1993).

In conclusion, the model presented here provides several advantages for the representation of both the microscopic and macroscopic properties of ionotropic receptors. Nevertheless, caution should be exercised in future applications. Only four states have been utilized and it is possible that additional states will be required for the modelling of certain competitive antagonists, as well as the characterization of new mutant forms. Furthermore, the simplification that permitted reducing the full tetrahedral model to the linear cascade (Fig. 1) may not be applicable in all cases. For example, the initial single-channel measurements with the $\alpha 7$ mutant L247T (Revah et al. 1991) suggest that a direct $B \rightleftharpoons I$ transition may be required. In general, additional information is potentially available with current experimental techniques for fast chemical kinetics and electrophysiological recordings to render the diverse assumptions of the model amenable to experimental test. Ultimately, it will be of interest to explore the extent to which similar modelling can be applied to the ligand-gated receptors for other classes of neurotransmitters.

Appendix. Equilibrium equations for ligand binding and change of state

For the four-state allosteric model, ($\bar{Y}_4$), a global ligand-binding function, and ($\bar{D}$), the fractional occupancy of the D state (or equivalent fractional occupancy equations for the B, A or I states) may be defined as follows:

$$\bar{Y}_4 = \frac{\alpha_D(1+\alpha_D)^{N-1} + {}^{ID}L_0\,{}^{ID}c\alpha_D(1+{}^{ID}c\alpha_D)^{N-1} + {}^{AD}L_0\,{}^{AD}c\alpha_D(1+{}^{AD}c\alpha_D)^{N-1} + {}^{BD}L_0\,{}^{BD}c\alpha_D(1+{}^{BD}c\alpha_D)^{N-1}}{(1+\alpha_D)^N + {}^{ID}L_0(1+{}^{ID}c\alpha_D)^N + {}^{AD}L_0(1+{}^{AD}c\alpha_D)^N + {}^{BD}L_0(1+{}^{BD}c\alpha_D)^N} \quad \text{(A1)}$$

$$\bar{D} = \frac{(1+\alpha_D)^N}{(1+\alpha_D)^N + {}^{ID}L_0({}^{1}+{}^{ID}c\alpha_D)^N + {}^{AD}L_0(1+{}^{AD}c\alpha_D)^N + {}^{BD}L_0(1+{}^{BD}c\alpha_D)^N} \quad \text{(A2)}$$

In these equations N is the number of ligand (agonist) binding sites per receptor molecule (two for the applications presented here), α_D is the concentration of ligand (X) normalized to the affinity of the D state ($\alpha_D = [X]/{}^{D}K_d$), and four composite constants are utilized (${}^{AD}L_0 = {}^{ID}L_0\,{}^{AI}L_0$; ${}^{BD}L_0 = {}^{ID}L_0\,{}^{AI}L_0\,{}^{BA}L_0$; ${}^{AD}c = {}^{ID}c\,{}^{AI}c$; ${}^{BD}c = {}^{ID}c\,{}^{AI}c\,{}^{BA}c$). For the simulation of dose-response curves and their relation to ligand binding involving the $B \leftrightarrow A$ transitions, the fractional ligand binding ($\bar{Y}_{BA}$) and fractional occupancy of the A state ($\bar{A}$) are defined as:

$$\bar{Y}_{BA} = \frac{\alpha_A(1+\alpha_A)^{N-1} + {}^{BA}L_0\,{}^{BA}c\alpha_A(1+{}^{BA}c\alpha_A)^{N-1}}{(1+\alpha_A)^N + {}^{BA}L_0(1+{}^{BA}c\alpha_A)^N} \quad \text{(A3)}$$

$$\bar{A} = \frac{(1+\alpha_A)^N}{(1+\alpha_A)^N + {}^{BA}L_0(1+{}^{BA}c\alpha_A)^N} \quad \text{(A4)}$$

In this case α_A is the concentration of ligand (X) normalized to the affinity of the A state:

$$\alpha_A = (X)/{}^{A}K_d.$$

The apparent affinity for ligand binding predicted by the allosteric formulation, in terms of the normalized agonist concentration at half-maximal saturation, ${}^{Y}\alpha_{1/2}$, is given (for $N = 2$) by the equation: $({}^{Y}\alpha_{1/2})^2 = (1+{}^{BA}L_0)/(1+{}^{BA}L_2)$, with a value of ${}^{Y}\alpha_{1/2} = 139.8$ for parameters of Table 1. The value of ${}^{Y}\alpha_{1/2}$, may also be closely approximated by the simplified relationship: ${}^{Y}\alpha_{1/2} = \sqrt{{}^{BA}L_0}$ (Edelstein 1971), yielding in this case ${}^{Y}\alpha_{1/2} = 141.4$. However, under these conditions, since ${}^{BA}L_0 > 1/{}^{BA}c$, the change of state function ($\bar{A}_{norm}$) lies slightly to the right of the ligand binding function $\bar{Y}_{BA}$, such that ${}^{A}\alpha_{1/2} \sim 160$, which corresponds to the EC_{50} of a dose-response curve with a value of $EC_{50} = {}^{A}\alpha_{1/2}\,{}^{A}K_d = 8\ \mu M$.

Although electrophysiological measurements that monitor channel opening will reflect $\bar{A}$, it may be possible in some cases to obtain parallel data for $\bar{Y}_{BA}$. It is therefore important to note fundamental differences that may occur in the two measurements. Whereas $\bar{Y}_{BA}$ always varies from 0 to 1 as a function of α, the values of $\bar{A}$ are limited to the range between $\bar{A}_{min}$ at $\alpha_A = 0$ and $\bar{A}_{max}$ at

$\alpha_A = \infty$, where

$$\bar{A}_{min} = \frac{1}{1 + {}^{BA}L_0} \quad \text{and} \quad \bar{A}_{max} = \frac{1}{1 + {}^{BA}L_0({}^{BA}c)^N} \tag{A5}$$

However, for experimental data, the minimal and maximal signals define a range between 0 and 1, which corresponds to a normalized function, $\bar{A}_{norm}$:

$$\bar{A}_{norm} = \frac{\dfrac{(1+\alpha_A)^N}{(1+\alpha_A)^N + {}^{BA}L_0(1+{}^{BA}c\alpha_A)^N} - \bar{A}_{min}}{\bar{A}_{max} - \bar{A}_{min}} \tag{A6}$$

The denominator of (A6) is equivalent to what has been designated the 'allosteric range' (Rubin and Changeux 1966).

The cooperative behavior may be related to the allosteric equations for the binding or state functions. For a given set of allosteric parameters (N sites and discrete values of ${}^{BA}L_0$, and ${}^{BA}c$), the cooperativity is defined independently for the binding and change of state functions in terms of distinct Hill coefficients, $n_{H,Y}$ and $n_{H,A}$, obtained as the slope of the corresponding 'Hill plot':

$$n_{H,Y} = \frac{d\log[\bar{Y}_{BA}/(1-\bar{Y}_{BA})]}{d\log\alpha_A} \tag{A7}$$

$$n_{H,A} = \frac{d\log[\bar{A}_{norm}/(1-\bar{A}_{norm})]}{d\log\alpha_A} \tag{A8}$$

Although an average Hill coefficient can be obtained from the slope of a linear fitting over an entire response range, it is instructive to note that the Hill coefficient is not constant as a function of ligand concentration. The changes in the slopes, corresponding to variations in $n_{H,Y}$ and $n_{H,A}$, may be plotted as a function of log $[\bar{Y}_{BA}/(1-\bar{Y}_{BA})]$ to permit the behaviour at the extremes of saturation to be more readily visualized. The average Hill coefficient ($\bar{n}_H$) may also be defined with the non-linear empirical equation often used to fit dose-response data:

$$\bar{A}_{norm} = \left(\frac{[X]}{EC_{50} + [X]}\right)^{\bar{n}_H} \tag{A9}$$

or by evaluating $\bar{n}_H$ directly from the slope of the log-log plot at low [X]. However, the approximation permitting $\bar{n}_H$ to be obtained from the slope of the log-log plot is only valid for very low values of α, corresponding in the example presented to $\bar{A}_{norm} < 0.01$.

With two sites (N = 2), the maximum value of $n_{H,Y}$ occurs under all conditions at precisely $\bar{Y}_{BA} = 0.5$, whereas the maximum value of $n_{H,A}$ is obtained at a value of $\bar{A}_{norm} = 1/[1 + {}^{BA}L_0\ ({}^{BA}c)^{N/2}]$. However, when the condition for symmetrical curves, ${}^{BA}L_0 = ({}^{BA}c)^{-N/2}$, is satisfied, maxima for both $n_{H,Y}$ and $n_{H,A}$ occur at $\bar{Y}_{BA} = 0.5$ and $\bar{A} = 0.5$ regardless of the number of binding sites. In this case, with N = 2, the curves for $\bar{A}_{norm}$ and $\bar{Y}_{BA}$ overlap fully, since (A3) and (A6) simplify to a common form:

$$\bar{Y}_{BA} = \bar{A}_{norm} = \frac{\alpha(2{}^{BA}L_0 + {}^{BA}L_0\alpha + \alpha)}{{}^{BA}L_0 + 4{}^{BA}L_0\alpha + {}^{BA}L_0(\alpha)^2 + ({}^{BA}L_0)^2 + (\alpha)^2} \tag{A10}$$

For values of N = 3 or greater, curves for $\bar{A}_{norm}$ and $\bar{Y}_{BA}$ are always distinct, even under conditions of symmetry, and diverge progressively as N increases: $\bar{A}_{norm}$ changes more abruptly than $\bar{Y}_{BA}$, since the $\bar{A}_{norm}$ values are below $\bar{Y}_{BA}$ at low α and above $\bar{Y}_{BA}$ at high α, thereby explaining why $n_{H,A} > n_{H,Y}$ at all degrees of ligand binding.

Although the divergence between $\bar{A}_{norm}$ and $\bar{Y}_{BA}$ is particularly marked at the extremes, experimental measurements may readily be made in this range. For example, Franke et al. (1993) report dose-response data at fractional responses of less than 0.001 and measurements in this range could provide important distinctions between binding and change of state functions, were data obtained in parallel available, for example using a fluorescent agonist (see Changeux and Edelstein 1994). With respect to desensitization measured by pre-pulses of low concentration, the determination of IC_{50} values may be related to the state function, $\bar{D}$ (A2), using a normalized form equivalent to (A6):

$$\bar{D}_{norm} = \frac{\dfrac{(1+\alpha_D)^N}{(1+\alpha_D)^N + {}^{ID}L_0(1+{}^{ID}c\alpha_D)^N + {}^{AD}L_0(1+{}^{AD}c\alpha_D)^N + {}^{BD}L_0(1+{}^{BD}c\alpha_D)^N} - \bar{D}_{min}}{\bar{D}_{max} - \bar{D}_{min}} \tag{A11}$$

where

$$\bar{D}_{min} = \frac{1}{1 + {}^{ID}L_0 + {}^{AD}L_0 + {}^{BD}L_0}$$

and

$$\bar{D}_{max} = \frac{1}{1 + {}^{ID}L_0({}^{ID}c)^N + {}^{AD}L_0({}^{AD}c)^N + {}^{BD}L_0({}^{BD}c)^N} \tag{A12}$$

and other constants are defined in relation to (A2). Equation (A11), in the form $(1 - \bar{D}_{norm})$, corresponds to the type of data used in the determination of IC_{50} values (Fig. 9).

Acknowledgements. This research was supported by the Swiss National Science Foundation and OFES, the Human Frontiers Science Program, and the following French sources: the Centre National de la Recherche Scientifique, the Collège de France and the Direction des Recherches Etudes et Techniques. We thank Attila Szabo, Jean-Luc Galzi and Clement Lena for helpful discussions. S.J.E. gratefully acknowledges an EMBO Short-Term Fellowship.

References

Adelsberger-Mangan DM, Levy WB (1994) The influence of limited presynaptic growth and synapse removal on adaptive synaptogenesis. Biol Cybern 71:461–468

Amit DJ (1989) Modeling brain functions. Cambridge University Press, Cambridge

Auerbach A (1993) A statistical analysis of acetylcholine receptor activation in *Xenopus* myocytes: stepwise versus concerted models of gating. J Physiol (Lond) 461:339–378

Bartol TM, Land BR, Salpeter EE, Salpeter MM (1991) Monte Carlo simulation of miniature endplate current generation in the vertebrate neuromuscular junction. Biophys J 59:1290–1307

Bekkers JM (1994) Quantal analysis of synaptic transmission in the central nervous system. Curr Opin Neurobiol 4:360–365

Bertrand D, Bader CR, Distasi C, Forster IC (1989) Single-channel current simulation and recording using a photodiode as current generator. J Neurosci Methods 26:233–238

Bertrand D, Devillers-Thiéry A, Revah F, Galzi J-L, Hussy N, Mulle C, Bertrand S, Ballivet M, Changeux J-P (1992) Unconventional pharmacology of a neural nicotinic receptor mutated in the channel domain. Proc Natl Acad Sci USA 89:1261–1265

Bertrand D, Galzi J-L, Devillers-Thiéry A, Bertrand S, Changeux J-P (1993) Mutations at two distinct sites within the channel domain M2 alter calcium permeability of neuronal a7 nicotinic receptor. Proc Natl Acad Sci USA 90:6971–6975

Bienenstock EL, Cooper LN, Munro PW (1982) Theory for the development of neuron selectivity: orientation specificity and binocular interaction in visual cortex. J Neurosci 2:32–48

Blanton MP, Cohen JB (1994) Identifying the lipid-protein interface of the *Torpedo* nicotinic acetylcholine receptor: secondary structure implications. Biochemistry 33:2859–2872

Boyd ND, Cohen JB (1980) Kinetics of binding of [^{3}H]acetylcholine and [^{3}H]carbamoylcholine to *Torpedo* postsynaptic membranes: slow conformational transitions of the cholinergic receptor. Biochemistry 19:5344–5353

Buonomano DV, Merzenich MM (1995) Temporal information transformed into a spatial code by a neural network with realistic properties. Science 267:1028–1030

Chang HW, Bock E (1977) Molecular forms of acetylcholine receptor: effects of calcium ions and a sulfhydryl reagent on the occurrence of oligomers. Biochemistry 16:4513–4520

Changeux J-P (1990) Functional architecture and dynamics of the nicotinic acetylcholine receptor: an allosteric ligand-gated channel. In: Changeux J-P, Llinas RR, Purves D, Bloom FF (eds) Fidia Research Foundation Neurosciences Award Lectures, vol 4. Raven Press, New York, pp 17–168

Changeux J-P (1993) A critical view of neuronal models of learning and memory. In: Anderson P, Hvalby O, Paulsen O, Hokfelt B (eds) Memory concepts—1993. Basic and clinical aspects. Elsevier, Amsterdam, pp 413–433

Changeux J-P, Dehaene S (1989) Neuronal models of cognitive functions. Cognition 33:63–109

Changeux J-P, Edelstein SJ (1994) On allosteric transitions and acetylcholine receptors. Trends Biochem Sci 19:399–340

Changeux J-P, Heidmann T (1987) Allosteric receptors and molecular models of learning. In: Edelman G, Gall WE, Cowan WM (eds) Synaptic function. Wiley, New York, pp 549–601

Changeux J-P, Rubin MM (1967) Allosteric interactions in aspartate transcarbamylase. III. Interpretations of experimental data in terms of the model of Monod, Wyman, and Changeux. Biochemistry 7:553–561

Changeux J-P, Thiéry J-P, Tung T, Kittel C (1967) On the cooperativity of biological membranes. Proc Natl Acad Sci USA 57:335–341

Changeux J-P, Galzi J-L, Devillers-Thiéry A, Bertrand D (1992) The functional architecture of the acetylcholine nicotinic receptor explored by affinity labeling and site-directed mutagenesis. Q Rev Biophys 25:395–432

Churchland PS, Sejnowski TJ (1992) The computational brain. MIT Press, Cambridge, Mass

Clements JD, Lester RAJ, Tong G, Jahr CE, Westbrook GL (1992) The time course of glutamate in the synaptic cleft. Science 258: 1498–1501

Colquhoun D, Hawkes AG (1977) Relaxations and fluctuations of membrane currents that flow through drug operated ion channels. Proc R Soc Lond B 199:231–262

Colquhoun D, Sakmann B (1985) Fast events in single-channel currents activated by acetylcholine and its analogues at the frog muscle end-plate. J Physiol (Lond) 369:501–557

Colquhoun D, Jonas P, Sakmann B (1992) Action of brief pulses of glutamate on AMPA/kainate receptors in patches from different neurones of rat hippocampal slices. J Physiol (Lond) 458:261–287

Cox DR, Miller HD (1965) The theory of stochastic processes. Chapman and Hall, London

Dehaene S, Changeux J-P (1991) The Wisconsin card sorting test: theoretical analysis and modeling in a neuronal network. Cerebral Cortex 1:62–79

Dehaene S, Changeux J-P, Nadal J-P (1987) Neural networks that learn temporal sequences by selection. Proc Natl Acad Sci USA 84:2727–2731

del Castillo J, Katz B (1957) Interaction at endplate receptors between different choline derivatives. J Physiol (Lond) 146:369–381

Dionne VE, Steinbach JH, Stevens CF (1978) An analysis of the dose-response relationships at voltage-clamped frog neuromuscular junctions. J Physiol (Lond) 281:421–444

Eaton WA, Henry ER, Hofrichter J (1991) Application of linear free energy relations to protein conformational changes: the quaternary structural change of hemoglobin. Proc Natl Acad Sci USA 88: 4472–4475

Edelman GM, Reeke GN, Gall WE, Tononi G, Williams D, Sporns O (1992) Synthetic neural modeling applied to a real-world artifact. Proc Natl Acad Sci USA 89:7267–7271

Edelstein SJ (1971) Extensions of the allosteric model for hemoglobin. Nature 230:224–227

Edelstein SJ (1972) An allosteric mechanism for the acetylcholine receptor. Biochem Biophys Res Commun 48:1160–1165

Edelstein SJ (1975) Cooperative interactions of hemoglobin. Annu Rev Biochem 44:209–232

Faber DS, Young WS, Legendre P, Korn H (1992) Intrinsic quantal variability due to stochastic properties of receptor-transmitter interactions. Science 258:1494–1498

Fersht AR, Leatherbarrow RJ, Wells TNC (1986) Quantitative analysis of structure-activity relationships in engineering proteins by linear free-energy relationships. Nature 322:284–286

Finkel LH, Edelman GM (1985) Interactions of synaptic modification rules within populations of neurons. Proc Natl Acad Sci USA 82:1291–1295

Foldiak P (1990) Forming sparse representations by local anti-Hebbian learning. Biol Cybern 64:165–170

Franke C, Parnas H, Hovav G, Dudel J (1993) A molecular scheme for the reaction between acetylcholine and nicotinic channels. Biophys J 64:339–356

Frenkel D (1993) Monte Carlo simulations: a primer. In: van Gunsteren WF, Weiner PK, Wilkinson AJ (eds) Computer simulation of biomolecular systems: theoretical and experimental applications, vol 2. ESCOM, Leiden, pp 37–66

Fuxe K, Agnati L (1991) Two principal modes of electro-chemical communication in the brain: volume versus wiring transmission. In: Fuxe K, Agnati L (eds) Volume transmission in the brain: novel mechanisms for neural transmission. Raven Press, New York, pp 1–9

Galzi J-L, Changeux J-P (1994) Neurotransmitter-gated ion channels as unconventional allosteric proteins. Curr Opin Struct Biol 4:554–565

Gouzé J-L, Lasry J-M, Changeux J-P (1983) Selective stabilization of muscle innervation during development: a mathematical model. Biol Cybern 46:207–215

Hangartner RD, Cull P (1996) A ternary logic model for recurrent neuromine networks with delay. Biol Cybern 73:177–188

Hebb DO (1949) The organization of behavior. Wiley, New York

Heidmann T, Changeux J-P (1978) Structural and functional properties of the acetylcholine receptor protein in its purified and membrane-bound states. Annu Rev Biochem 47:317–357

Heidmann T, Changeux J-P (1979) Fast kinetic studies on the interaction of a fluorescent agonist with the membrane-bound acetylcholine receptor from *Torpedo marmorata*. Eur J Biochem 94:255–279

Heidmann T, Changeux J-P (1980) Interaction of a fluorescent agonist with the membrane-bound acetylcholine receptor from *Torpedo marmorata* in the millisecond time range: resolution of an 'intermediate' conformational transition and evidence for positive cooperative effects. Biochem Biophys Res Commun 97:889–896

Heidmann T, Changeux J-P (1982) Un modèle moléculaire de régulation d'efficacité au niveau postsynaptique d'une synapse chimique. C R Acad Sci Paris 295:665–670

Herz A, Sulzer B, Kuhn R (1989) Hebbian learning reconsidered: representation of static and dynamic objects in associative neural nets. Biol Cybern 60:457–467

Hestrin S (1993) Different glutamate receptor channels mediate fast excitatory synaptic currents in inhibitory and excitatory cortical neurons. Neuron 11:1083–1091

Hopfield JJ (1995) Pattern recognition computation using action potential timing for stimulus representation. Nature 376:33–36

Huganir RL, Greengard P (1990) Regulation of neurotransmitter receptor desensitization by protein phosphorylation. Neuron 5:555–567

Huganir RL, Delcour AJ, Greengard P, Hess GP (1986) Phosphorylation of the nicotinic acetylcholine receptor regulates its rate of desensitization. Nature 321:774–776

Jackson MB (1986) Kinetics of unliganded acetylcholine receptor channel gating. Biophys J 49:663–672

Jackson MB (1988) Dependence of acetylcholine receptor channel kinetics on agonist concentration in cultured mouse muscle fibers. J Physiol (Lond) 397:555–583

Jackson MB (1989) Perfection of a synaptic receptor: kinetics and energetics of the acetylcholine receptor. Proc Natl Acad Sci USA 86:2199–2203

Jencks WP (1985) A primer for the Bema Hapothle. An empirical approach to the characterization of changing transition-state structures. Chem Rev 85:511–527

Kanai Y, Smith CP, Hediger MA (1993) The elusive transporters with a high affinity for glutamate. Trends Neurosci 16:365–370

Karlin A (1967) On the application of 'a plausible model' of allosteric proteins to the receptor of acetylcholine. J Theor Biol 16:306–320

Karlin A (1991) Explorations of the nicotinic acetylcholine receptor. Harvey Lect 85:71–107

Katz B, Miledi R (1977) Transmitter leakage from motor nerve endings. Proc R Soc Lond B 1996:59–72

Katz B, Thesleff S (1957) A study of 'desensitization' produced by acetylcholine at the motor end-plate. J Physiol (Lond) 138:83–80

Kerszberg M, Masson C (1995) Signal-induced selection among spontaneous oscillatory patterns in a model honeybee olfactory glomeruli. Biol Cybern 72:487–495

Kerszberg M, Zippelius A (1990) Synchronization in neural assemblies. Phys Scripta T33:54–64

Korn SJ, Horn R (1991) Discrimination of kinetic models of ion channel gating. In: Conn PM (ed) Electrophysiology and microinjection. Academic Press, San Diego, pp 428–456

Koshland DE, Némethy G, Filmer D (1966) Comparison of experimental binding data and theoretical models in proteins containing subunits. Biochemistry 5:365–385

Kuffler SW, Yoshikami D (1975) The distribution of acetylcholine sensitivity at the post-synaptic membrane of vertebrate skeletal twitch muscles: iontophoretic mapping in the micron range. J Physiol (Lond) 244:703–730

Leffler JE (1953) Parameters for the description of transition states. Science 117:340–341

Levitan IB (1994) Modulation of ion channels by protein phosphorylation and dephosphorylation. Annu Rev Physiol 56:193–212

Léna C, Changeux J-P (1993) Allosteric modulations of the nicotinic acetylcholine receptor. Trends Neurosci 16:181–186

Lingle CJ, Maconochie D, Steinbach JH (1992) Activation of skeletal muscle nicotinic acetylcholine receptors. J Membrane Biol 126:195–217

Lukas RJ, Bencherif M (1992) Heterogeneity and regulation of nicotinic acetylcholine receptors. Int Rev Neurobiol 34:25–131

Magleby KL, Pallotta BS (1981) A study of desensitization of acetylcholine receptors using nerve-released transmitter in the frog. J Physiol (Lond) 316:225–250

Magleby KL, Stevens CF (1972) A quantitative description of end-plate currents. J Physiol (Lond) 223:173–197

Matsubara N, Billington AP, Hess GP (1992) How fast does an acetylcholine channel open? Laser-pulse photolysis of an inactive precursor of carbamoylcholine in the microsecond time region with BC_3H1 cells. Biochemistry 31:5507–5514

McCulloch WS, Pitts W (1943) A logical calculus of the ideas imminent in nervous activity. Bull Math Biophys 5:115–137

Monod J, Wyman J, Changeux J-P (1965) On the nature of allosteric transitions: a plausible model. J Mol Biol 12:88–118

Montague PR, Sejnowski TJ (1994) The predictive brain: temporal coincidence and temporal order in synaptic learning mechanisms. Learn Mem 1:1–33

Mulle C, Léna C, Changeux J-P (1992) Potentiation of nicotinic receptor response by external calcium in rat central neurons. Neuron 8:937–945

Neubig RR, Cohen JB (1980) Permeability control by cholinergic receptors in *Torpedo* post-synaptic membranes: agonist dose-response relations measured at second and millisecond times. Biochemistry 19:2770–2779

Ochoa ELM, Li L, McNamee MG (1990) Desensitization of central cholinergic mechanisms and neuroadaptation to nicotine. Mol Neurobiol 4:251–287

Perutz MF (1989) Mechanisms of cooperativity and allosteric regulation in proteins. Q Rev Biophys 22:139–236

Petzold LR (1983) Automatic selection of methods for solving stiff and nonstiff systems of ordinary differential equations. J Sci Stat Comput 4:136–148

Press WH, Flannery BR, Teukolshy SA, Vetterling WT (1986) Numerical recipes. Cambridge University Press, Cambridge

Prinz H, Maelicke A (1992) Ligand binding to the membrane-bound acetylcholine receptor from *Torpedo marmorata*: a complete mathematical analysis. Biochemistry 31:6728–6738

Rang HP, Ritter JM (1970) On the mechanism of desensitization of cholinergic receptors. Mol Pharmacol 6:357–382

Revah F, Bertrand D, Galzi J-L, Devillers-Thiéry A, Mulle C, Hussy N, Bertrand S, Ballivet M, Changeux J-P (1991) Mutations in the channel domain alter desensitization of a neuronal nicotinic receptor. Nature 353:846–849

Role LW (1992) Diversity in primary structure and function of neuronal nicotinic acetylcholine receptor channels. Curr Opin Neurobiol 2:254–262

Rubin MM, Changeux J-P (1966) On the nature of allosteric transitions: implications of non-exclusive ligand binding. J Mol Biol 21:265–274

Sakmann B, Patlak J, Neher E (1980) Single acetylcholine-activated channels show burst-kinetics in presence of desensitizing concentrations of agonist. Nature 286:71–73

Sargent PB (1993) The diversity of neuronal nicotinic acetylcholine receptors. Annu Rev Neurosci 16:403–443

Sawicki CA, Gibson QH (1976) Quaternary conformational changes in human hemoglobin studied by laser photolysis of carboxyhemoglobin. J Biol Chem 251:1533–1542

Schachman HK (1988) Can a simple model account for the allosteric transition of aspartate transcarbamoylase? J Biol Chem 263:18583–18586

Shulman RG, Hopfield JJ, Ogawa S (1975) Allosteric interpretation of hemoglobin properties. Q Rev Biophys 8:325–420

Sine SM, Claudio T, Sigworth FJ (1990) Activation of *Torpedo* acetylcholine receptors expressed in mouse fibroblasts: single channel current kinetics reveal distinct agonist binding affinities. J Gen Physiol 96:395–437

Steinfeld JI, Francisco JS, Hase WL (1989) Chemical kinetics and dynamics. Prentice-Hall, Englewood Cliffs

Szabo A (1978) Kinetics of hemoglobin and transition state theory. Proc Natl Acad Sci USA 75:2108–2111

Trussell LO, Fischbach GD (1989) Glutamate receptor desensitization and its role in synaptic transmission. Neuron 3:209–218

Unwin N (1993) The nicotinic acetylcholine receptor at 9 Å resolution. J Mol Biol 229:1101–1124

Valenta DC, Downing JEG, Role LW (1993) Peptide modulation of ACh receptor desensitization controls neurotransmitter release from chicken sympathetic neurons. J Neurophysiol 69:928–942

Valera S, Ballivet M, Bertrand D (1992) Progesterone modulates a neuronal nicotinic acetylcholine receptor. Proc Natl Acad Sci USA 89:9949–9953

Wigstrom H, Gustafsson B (1985) On long-lasting potentiation in the hippocampus: a proposed mechanism for its dependence on coincident pre- and postsynaptic activity. Acta Physiol Scand 123:519–522

Wilson DL, Brown AM (1985) Effect of limited interval resolution on single channel measurements with application to Ca channels. IEEE Trans Biomed Eng 32:786–797

Wonnacott S (1990) The paradox of nicotinic acetylcholine receptor upregulation by nicotine. Trends Pharmacol Sci 11:216–219